GeoExpert ag

swiss*nuclear*: PEGASOS Refinement Project:
SP2 – Ground Motion Characterization

Contract no. PMT-VT-1032

Seismic Shear Wave Velocity Determination and Hybrid Seismic Survey at the SED-Station BRANT (Les Verrières, NE)

Date of Field Data Acquisition 19th May 2009

Report

Client

swiss*nuclear*
Project PRP
Frohburgstrasse 17
4601 Olten

Contractor

GeoExpert ag
Seismic Prospecting
Ifangstrasse 12b
P.O. Box 451
8603 Schwerzenbach

8603 Schwerzenbach, 3rd July 2009

INDEX

1 INTRODUCTION

1.1 Survey objectives

The seismic survey's main task is to provide information about the distribution function of the shear wave velocities in the depth interval of the uppermost 30 m along a 100 m long seismic profile.

Additionally, the following objectives are to be met:

- the mapping of the topography of the rock face, i.e. the thickness of the Quaternary deposits;
- the determination of the thickness of the weathered zone and its degree of decompaction at the bedrock surface;
- a general view of geological structures.

1.2 The choice of the appropriate surveying methods

Several methods are available for deriving the s-wave velocity distribution in the subsurface at any given position:

- in-situ measurement by down-hole or crosshole seismic surveying;
- shear-wave refraction tomography profiling;
- dispersion analysis of surface waves (MASW; **M**ultiple channel **A**nalysis of **S**urface **W**aves)

The surveys are to be carried out at, or as close as possible near some 20 SED earth quake monitoring stations in Switzerland. Ideally, the surveys are to be conducted on two orthogonal profiles in order to derive at their point of intersection a robust 1D s-wave velocity distribution function by correlation. To this end, the methods of MASW and shear-wave refraction tomography profiling are to be combined.

The results are to include the following fundamental parameters $v_{s,5}$, $v_{s,10}$, $v_{s,20}$, $v_{s,30}$, $v_{s,40}$, $v_{s,50}$, $v_{s,100}$ are to be calculated, also an error estimation of all values.

The data acquired for the MASW method are to be subjected to complementary **p-wave hybrid seismic data processing** in order to image the geological structures.

2 FIELD DATA ACQUISITION PARTICULARS

2.1 Time Schedule

Date	*Time*	*Activities / remarks*
19.05.2009	0750	arrival at site
	0750 - 0810	site reconnaissance
	0810 - 0910	lay-out of spread profile 1 (p-wave and s-wave)
	0910 - 0945	data acquisition of spread profile 1 (p-wave)
	1000 - 1050	data acquisition of spread profile 1 (s-wave)
	1050 - 1120	lay-out of spread profile 2 (p-wave and s-wave)
	1120 - 1205	data acquisition of spread profile 2 (p-wave)
	1205 - 1250	data acquisition of spread profile 2 (s-wave)
	1250 - 1430	removal of the seismic measuring system
	1430	leaving from site

2.2 Summary of Data Acquisition Parameters

Compressional Wave Data Acquisition

# of active channels	96
geophone type	4.5 Hz natural frequency, vertical velocimeter
receiver station spacing	1.0 m
# of geophones/station	1
source point spacing	2.0 m to 3.0 m
source type	vertical hammer (8 kg) striking on a horizontal metal plate
sampling rate	500 µs
recording time	2048 ms
field filters	0.5 Hz LC, anti-alias
# of field records	51 (line 09SN_06BRANT-P1) and 50 (line 09SN_06BRANT-P2)

Shear Wave Data Acquisition

# of active channels	48
geophone type	10 Hz natural frequency, horizontal velocimeter
receiver station spacing	2.0 m
# of geophones/station	1
source point spacing	4.0 m to 6.0 m
source type	horizontal hammer (8 kg) striking horizontally at a metal-plated wooden beam anchored to the ground by means of 20 cm long spikes
sampling rate	500 µs
recording time	512 ms
field filters	2 Hz LC, anti-alias
# of field records	51 (line 09SN_06BRANT-S1) and 50 (line 09SN_06BRANT-S2)

Fig. 2.1: S-wave data acquisition at profile 09SN_06BRANT-S1.

2.3 Composition of Seismic Field Crew

Personnel

Jochen Fiseli	Dipl.-Geologist, University of Freiburg i. Br., party chief
Fabian Isler	assistant, spread lay-out and activation of seismic source
Michael Kuhlmann	assistant, spread lay-out and activation of seismic source

Equipment

96	vertical geophones 4.5 Hz
48	horizontal geophones 12 Hz
6	seismic cables
1	seismic acquisition system Summit Compact, 96 channels
1	laptop computer for data acquisition
3	walkie-talkies
1	hammer 6 kg
1	steel plate
1	metal-plated wooden beam
1	van (FIAT Ducato 4x4)

2.4 Location

The seismic monitoring station BRANT (Les Verrières, Ne) is situated inside a cave, on the top of a Jurassic (Malm) karstified sediment plateau (Jura ridge) in Western Switzerland, canton of Neuchâtel.

Fig. 2.2: The red cross marked seismic monitoring station BRANT(Les Verrières, NE) is located in the Jurassic sediments (Malm) of Jura ridge. (map: geodata @ swisstopo).

2.5 Recording Conditions and Line Setup

Sunny weather and warm temperatures prevailed throughout the field data recording period. In general, the data quality obtained at BRANT is to be rated as good.

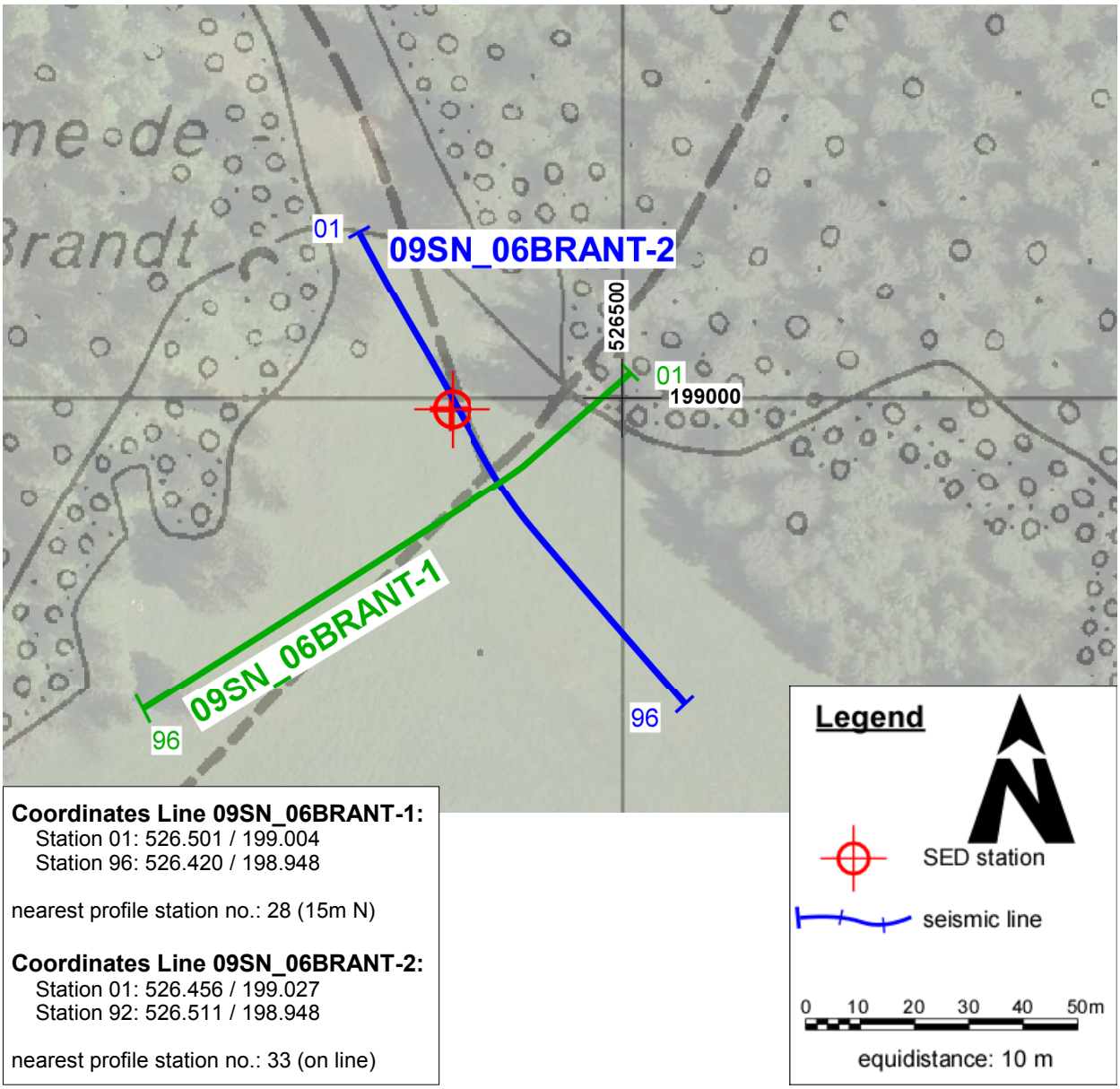

Fig. 2.3: Situation map with the trace of seismic profile 09SN_06BRANT-1 and -2. (background map: © SITN, Swisstopo (DV 571.4 & 2283.2) / Informations dépourvues de foi publique) Coordinates Line 09SN_06BRANT-1 and -2

3 SEISMIC DATA PROCESSING AND IMAGING OF THE RESULTS

3.1 General Remarks

- For the shear and compressional wave refraction seismic evaluation the package **RAYFRACT** by Intelligent Resources Ltd., Vancouver CAN, was used. The system features the technique of diving wave tomography (www.rayfract.com).
- The system **SPW** (**S**eismic **P**rocessing **W**orkshop) of Parallel Geoscience Corporation, Austin US-TX, was used for reflection seismic data processing (www.parallelgeo.com).
- Data processing of surface waves (MASW processing) was conducted with the software package **SurfSeis** V2.0 of Kansas Geological Survey in Lawrence US-KS.

A detailed description of the various surveying methods will be included in the general summary report.

3.2 Shear Wave Refraction Tomography

3.2.1 Reformatting and field geometry assignment

After reformatting the field data into the Rayfract format the field geometry is applied.

3.2.2 First break time picking

At each shot position, two seismic records were acquired in both activation directions. These two records are displayed superimposed with different colors on each other in Fig 3.2a together with the manually determined first arrival time picks.

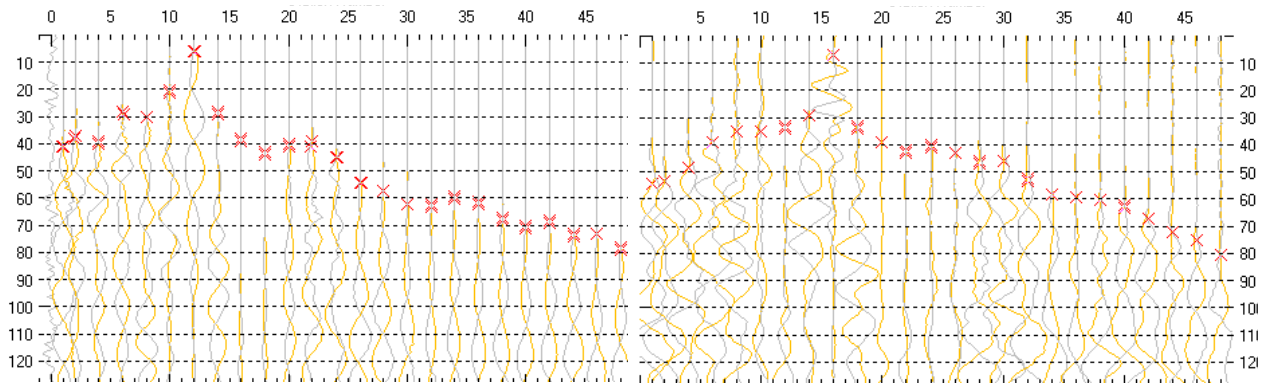

*Fig. 3.2a: High quality dual field record of line 09SN_06BRANT-S1 (left) and 09SN_06BRANTN-S2 (right).showing at each station the s-wave traces with opposing polarities in different colors. The manually picked s-wave refraction arrivals at each station are marked with an **x**. The station spacing is 2 m, profile station number 00 = profile meter 0; profile station number 48 = profile meter 96.*

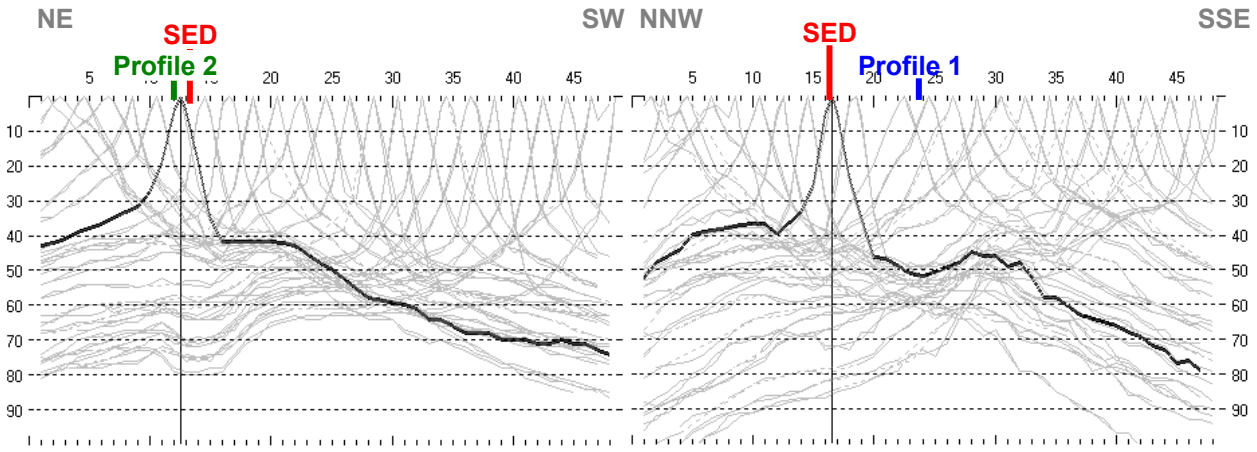

Fig. 3.2b: Curves of s-wave first break time picks of line 09SN_06BRANT-S1 (left) and 09SN_06BRANT-S2 (right).

3.2.3 Analytical Determination of Refraction Velocities

An initial 1D-velocity function (averaged 1D velocity-depth profiles derived by the Delta-t-V method, see Tab. 3.2a) is determined in the 3-dimensional time-offset-CMP-domain of all first break arrival time curves in the 3-dimensional time-offset-CMP-domain (see. Fig. 3.2c).

Depth [m]	Vs [m/s]
0.0	198
0.4	207
0.7	238
1.1	271
1.4	287
2.1	366
2.8	471
3.9	648
5.3	894
6.9	1175
9.2	1489
12.3	1816
16.0	1889
21.0	2678
27.4	3514
35.9	2347
46.7	3268

Depth [m]	Vs [m/s]
0.0	207
0.4	238
0.7	274
1.1	304
1.4	339
2.1	429
2.8	531
3.9	683
5.3	897
6.9	1094
9.2	1365
12.3	1719
16.0	2232
21.0	2583
27.4	2529
35.9	2524
46.7	2819

Tab. 3.2a: Initial 1D s-wave velocity function derived from real data of line 09SN_06BRANT-S1 (mean values between profile meters 24 and 55) and of line 09SN_06BRANT-S2 (mean values over all stations).

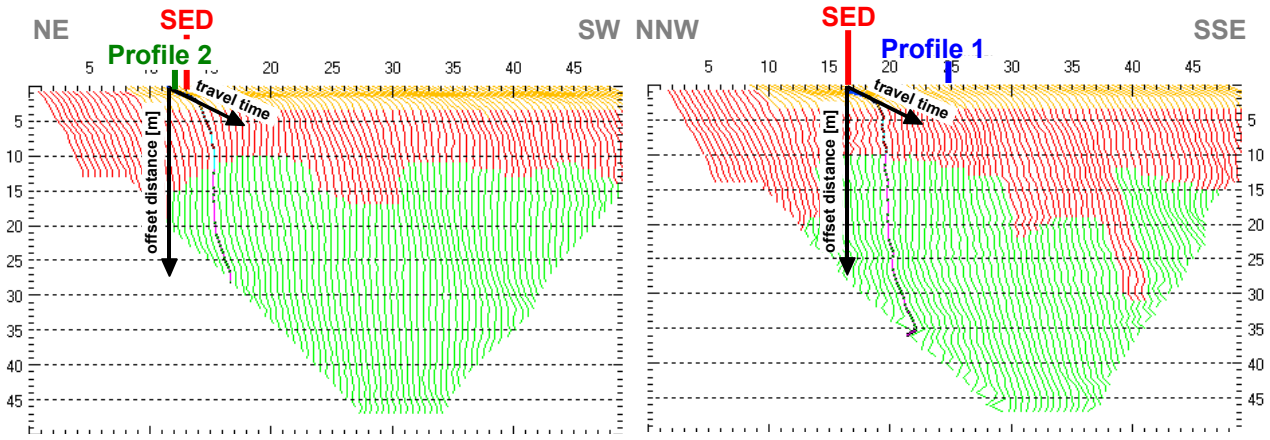

Fig. 3.2c: 3-dimensional distance-travel time diagrams of line 09SN_06BRANT-S1 (left) and 09SN_06BRANT-S2 (right) at the mid-points between source points and receiver stations are instrumental when using the analytical CMP derivation of the initial velocity field. The horizontal axes are the along the CMP positions and the travel time respectively, the vertical axis denotes the offset distance between source and receiver positions. The colors represent different velocity layers. The station spacing is 2 m, profile station number 00 = profile meter 0; profile station number 48 = profile meter 96. The colors represent different velocity layers.

3.2.4 Tomographic inversion of the velocity gradient field by iterative modeling

The velocity field is iteratively refined by the subsequent Wavepath Eikonal Traveltime (WET) tomographic inversion process. The inversion results are portrayed in Fig. 3.2d as a gridded velocity contour section and in Fig. 3.2e as a ray path density section.

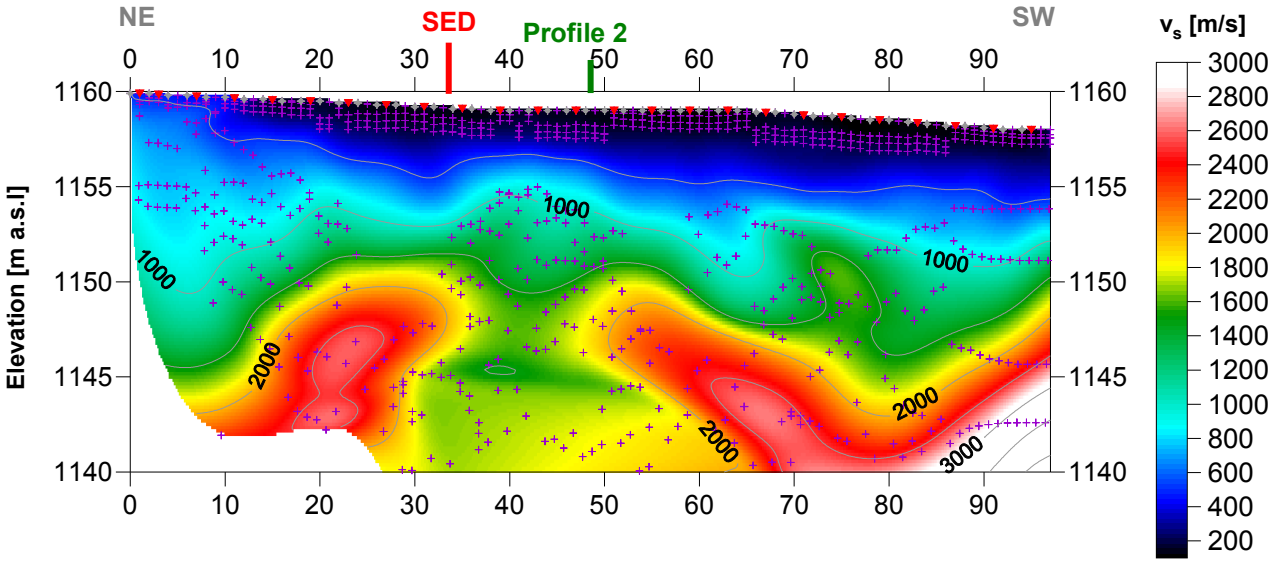

Fig. 3.2d: Shear wave velocity field of the line 09SN_06BRANT-S1. Red/white colors denote solid rock, blue/black colors point to unconsolidated sediments and soil. Vertical axis: elevation [m a.s.l]; horizontal axis: profile meter; color encoded scale: v_s [m/s]; vertical exaggeration: 2:1; gray diamonds: receiver positions; red triangles: source positions; magenta crosses: positions of determined velocity values. The station spacing is 2 m, profile meter 0 = profile station number 00, profile meter 96 = profile station number 48.

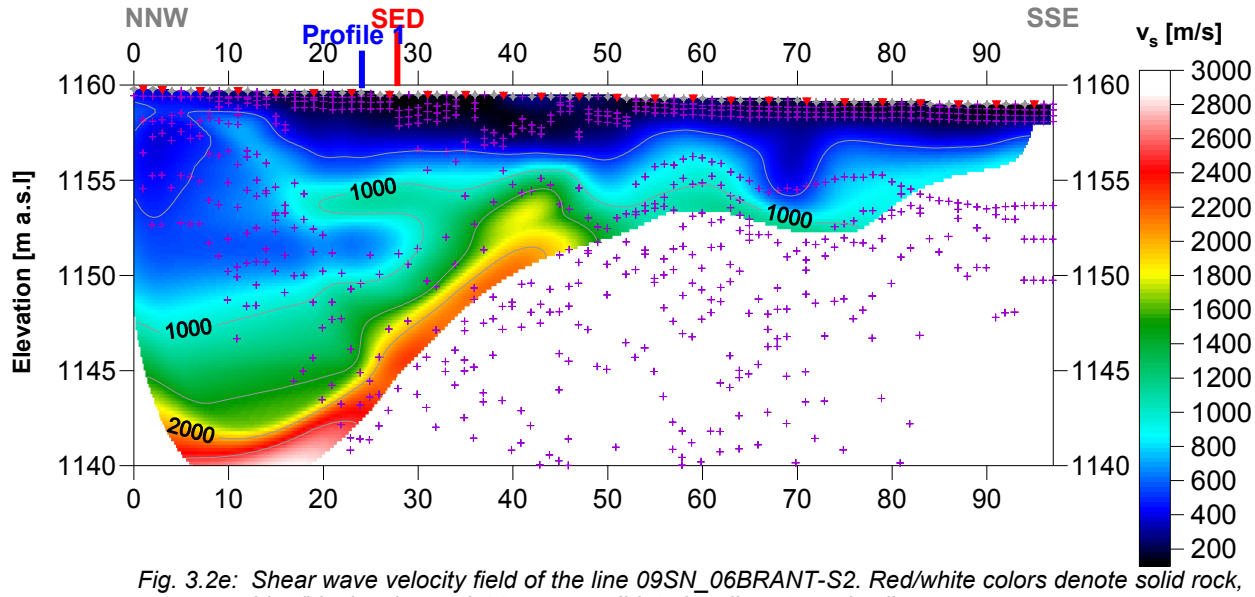

Fig. 3.2e: Shear wave velocity field of the line 09SN_06BRANT-S2. Red/white colors denote solid rock, blue/black colors point to unconsolidated sediments and soil.
Vertical axis: elevation [m a.s.l]; horizontal axis: profile meter; color encoded scale: v_s [m/s]; vertical exaggeration: 2:1; gray diamonds: receiver positions; red triangles: source positions; magenta crosses: positions of determined velocity values. The station spacing is 2 m.

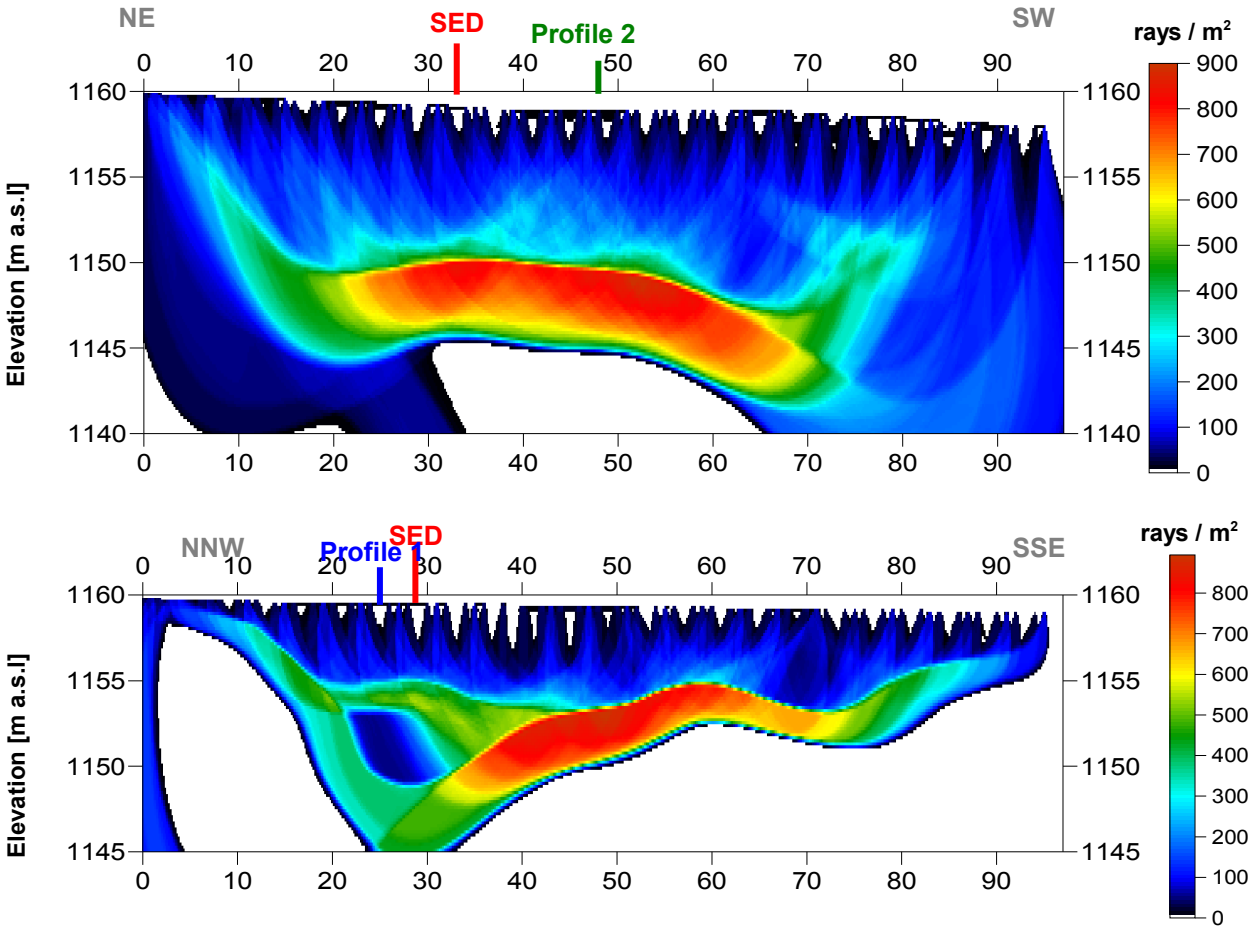

Fig. 3.2f: Shear wave ray path density along the seismic line 09SN_06BRANT-S1 (top) and -S2 (bottom). Red/white colors indicate high velocity contrasts (usually at the bedrock surface), blue/black colors denote low coverage areas. Vertical axis: elevation [m a.s.l]; horizontal axis: profile meter; color encoded scale: ray paths per m²; vertical exaggeration: 2:1. The station spacing is 2 m, profile meter 0 = profile station 00, profile meter 96 = profile station 48.

0.0	136
2.1	406
4.3	810
6.4	1174
8.5	1582
10.7	1890
12.8	1846
14.9	1769
17.1	1800
19.2	1786
21.3	1849
23.5	1993
25.6	2143
27.7	2274
29.9	2373
32.0	2498
34.1	2766
36.3	3043
38.4	3308

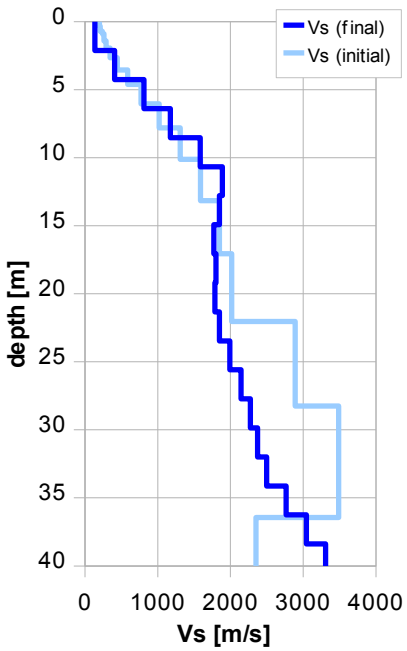

Tab. 3.2b: Final 1D s-wave velocity model derived from real data of line 09SN_06BRANT-S1 (horizontal average of all values) for the profile segment (between profile meters 25 and 50) with a geological setting resembling the one at the SED station. The calculated values of the initial 1D s-wave velocity model are given in Tab. 3.2a.

Depth [m]	Vs [m/s]
0.0	191
1.2	318
2.5	507
3.7	711
5.0	915
6.2	1044
7.5	1013
8.7	978
10.0	1072
11.2	1218
12.4	1324
13.7	1386
14.9	1522
16.2	1699
17.2	2020
18.5	2503
19.7	2873

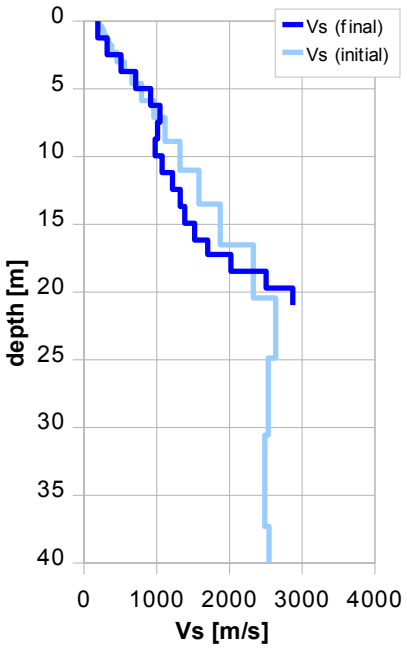

Tab. 3.2c: Final 1D s-wave velocity model derived from real data of line 09SN_06BRANT-S2 (horizontal average of all values) at the SED station. The calculated values of the initial 1D s-wave velocity model are given in Tab. 3.2a.

3.3 MASW Processing

3.3.1 Reformatting and field geometry assignment

The data preparation steps for the dispersion analysis include

- the assignment of the field acquisition geometry
- the selection of suitable offset ranges (=arrays) between 10 m and 50 m for dispersion, and the splitting of the field records in forward and reverse shooting direction data sets
- the reformatting of the data into the specific KGS format

X - - ... - - o-o-o-...-o-o-o (forward shooting or so-called PLUS direction)
respectively
o-o-o-...-o-o-o - - ... - - X (reverse shooting or so-called MINUS direction).

where **X** = shot position
o = receiver station
- = 1.0 m offset

The active array used at SED-station BRANT are the receiver station in the shot offset range between 10 and 50 m.

3.3.2 Calculating the dispersion image (overtone)

The result of dispersion analysis is the color encoded acoustic energy distribution in the phase velocity - frequency plane (see Fig. 3.3a and b).

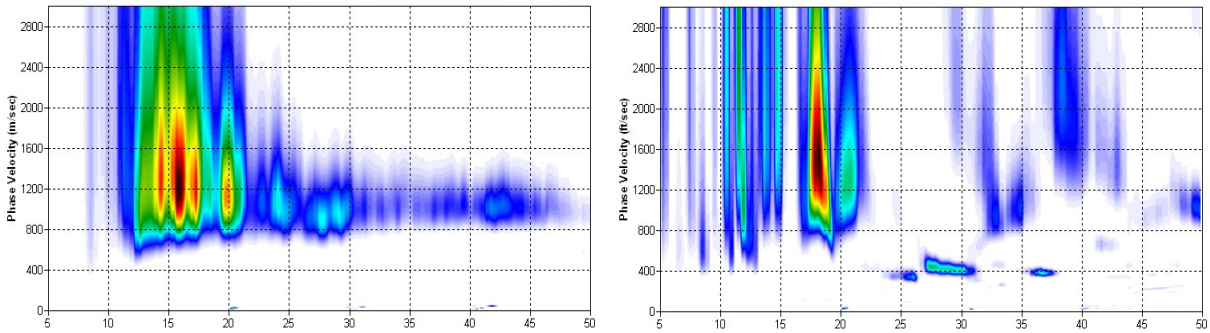

Fig. 3.3a: Dispersion image of fair to high quality data (left) 50 % and of deficient quality data (right) representing about 50 % of the MASW dataset of site BRANT. Horizontal axis: frequency from 5 to 50 Hz; vertical axis: phase velocity from 0 to 3000 m/s; color code: colors from white (no energy) to blue - green - yellow - red - black point to increasing energy amplitude values.

3.3.3 Analysis of the dispersion image

In the dispersion graphs as calculated in section 3.3.2 above, the curves joining the amplitude peaks of the fundamental modes are determined either by subjective inspection or in a semi-automated manner. On datasets with poorly defined amplitude peaks or with a highly irregular alignment of the peaks, the danger of obtaining improbable or wrong results is real and can only be mitigated by the processing experience and the a-priori knowledge of the geological setting by the geophysicist responsible for the data evaluation.

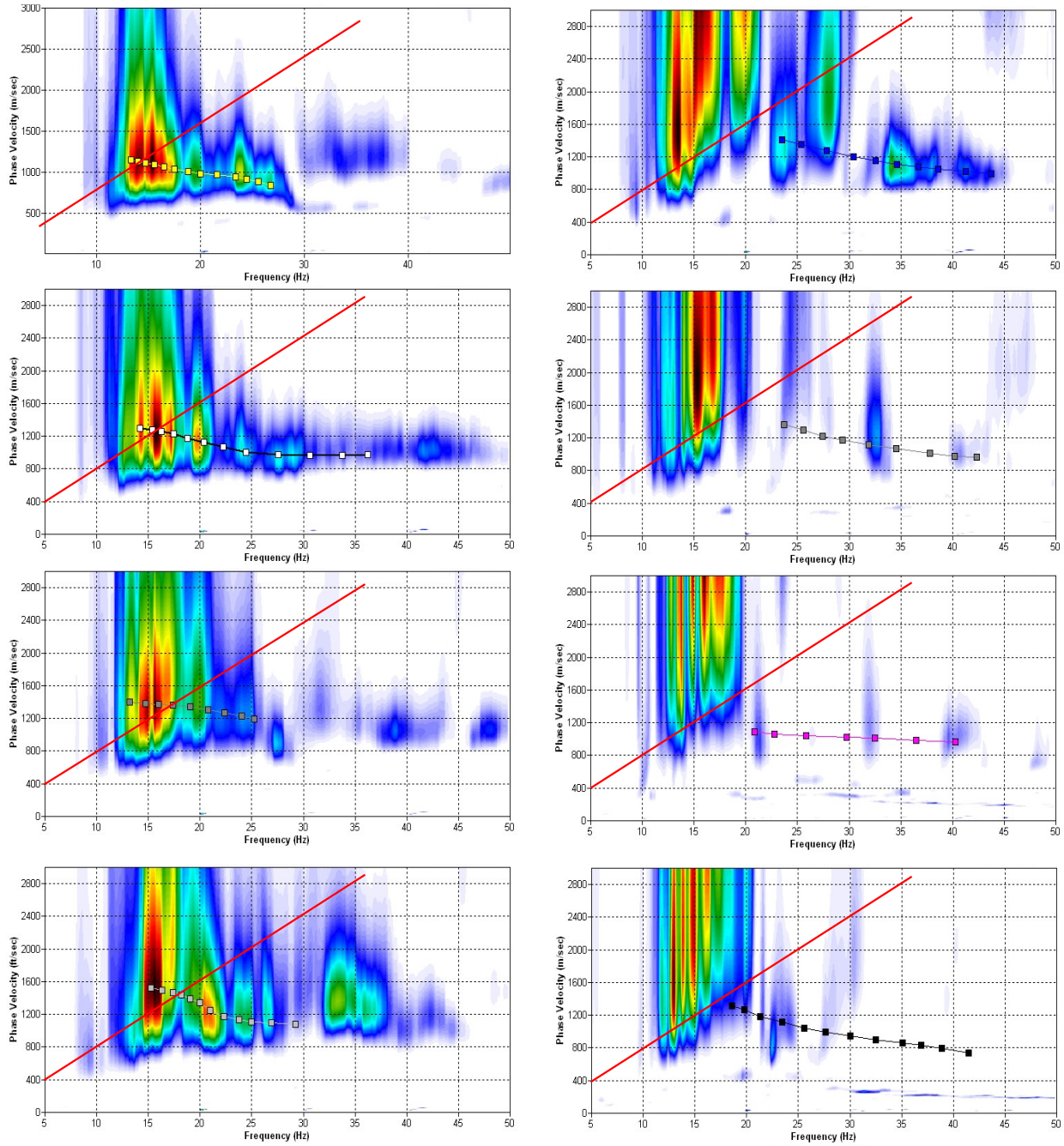

Fig. 3.3b: The manually picked dispersion images used for the derivation of the shear wave velocity section on line 09SN_06BRANT-M1. The dispersion curves (squares) are determined by linking the peaks of high energy. Note that 'higher modes' may at times produce higher energy peaks than the fundamental mode required for the analysis.
dotted fine line: signal-noise ratio for the designated f-v_{ph} – value.
red line: high resolution beam-forming curve for v_{max}.
1st row: left: station 25 @ PLUS direction; right: station 30 @ MINUS direction
2nd row: left: station 31 @ PLUS direction; right: station 36 @ MINUS direction
3rd row: left: station 39 @ PLUS direction; right: station 42 @ MINUS direction
4th row: left: station 47 @ PLUS direction; right: station 48 @ MINUS direction

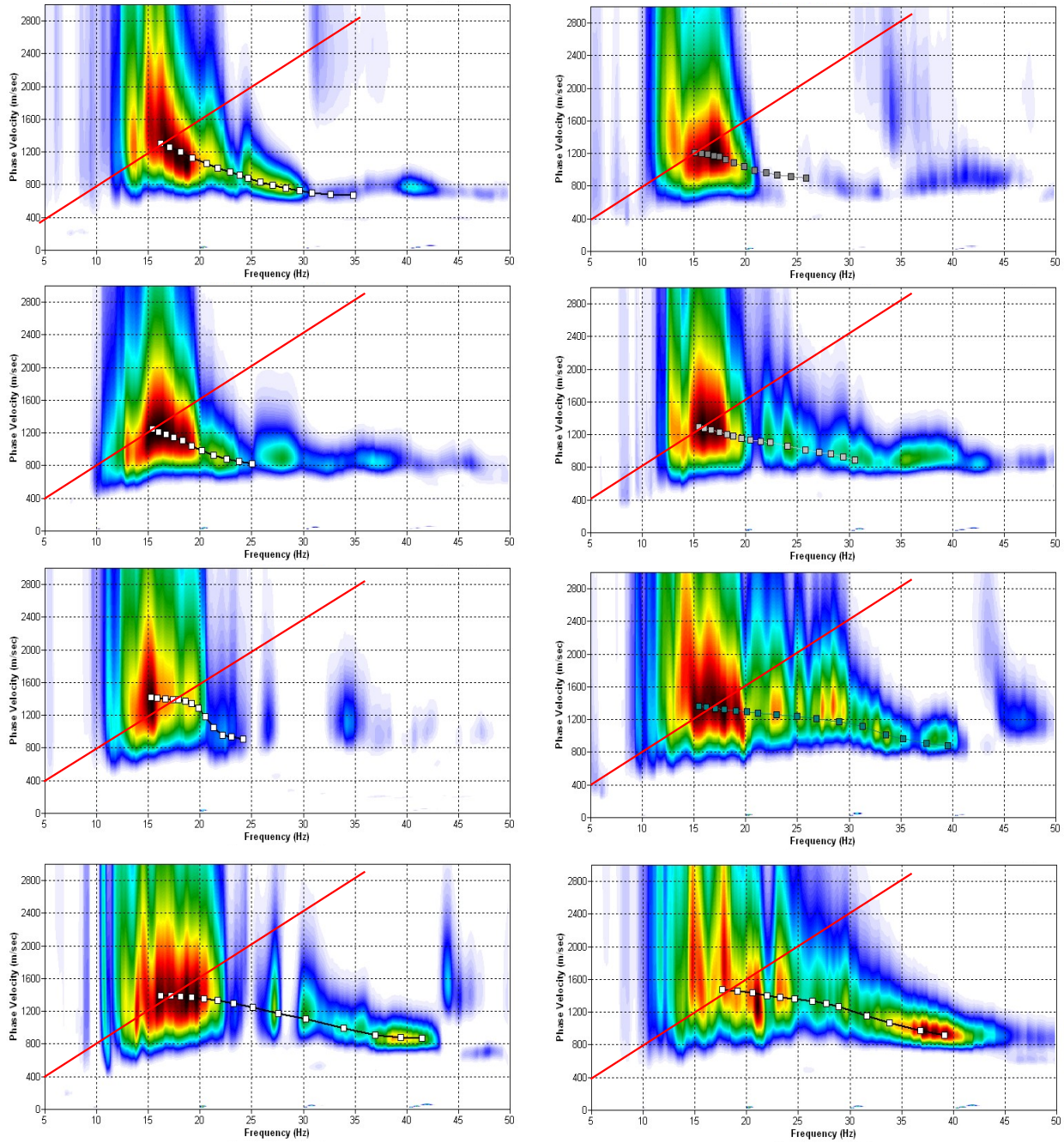

Fig. 3.3c: The manually picked dispersion images used for the derivation of the shear wave velocity section on line 09SN_01BRANT-M2. The dispersion curves (squares) are determined by linking the peaks of high energy. Note that 'higher modes' may at times produce higher energy peaks than the fundamental mode required for the analysis.
dotted fine line: signal-noise ratio for the designated f-v_{ph} – value.
red line: high resolution beam-forming curve for v_{max}.
1st row: left: station 25 @ PLUS direction; right: station 27 @ MINUS direction
2nd row: left: station 39 @ PLUS direction; right: station 42 @ MINUS direction
3rd row: left: station 54 @ PLUS direction; right: station 60 @ MINUS direction
4th row: left: station 75 @ PLUS direction; right: station 72 @ MINUS direction

3.3.4 Inversion of dispersion curves resulting in a 1D shear wave velocity distribution

Inversion of the extracted dispersion curves was performed using the algorithm described by Xia et al. (1999).

The inversion process is started by setting the maximum depth (z_{max}) to be in the order of 30% of the largest wavelength for an initial model consisting of 10 layers of increasing thicknesses. For all 10 layers the Poisson's ratio is assumed to be 0.4 and the rock/soil density to be 2.0 g/cm^3. The inversion process is concluded either after twelve iterations or when the convergence condition of a RMS-error of less than 3 m/s (phase velocity) is met.

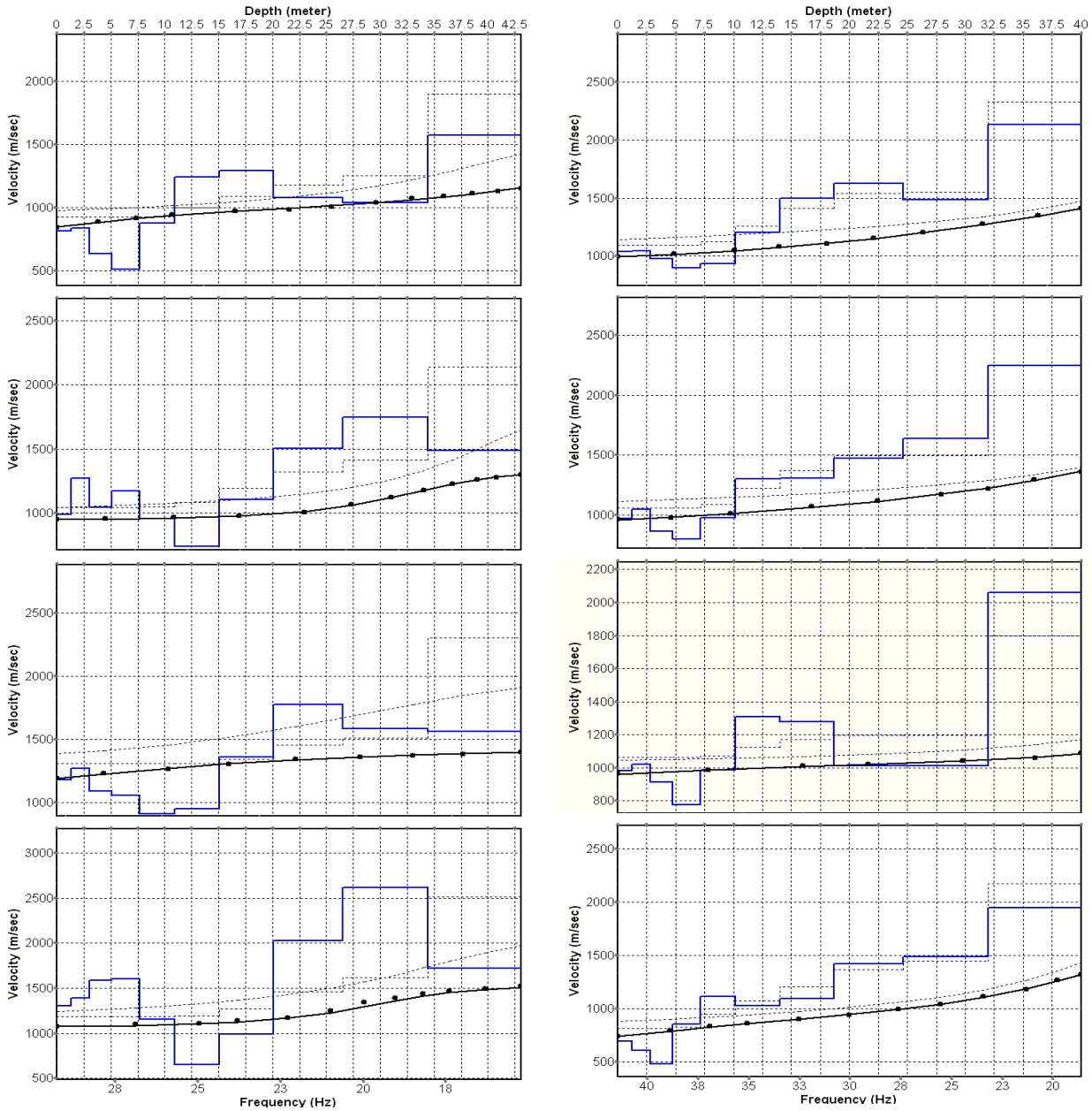

Fig. 3.3d: Inversion results of dispersion curves of dataset at line 09SN_06BRANT-M1.
***brown**: Inversion of dispersion curve (dots) resp. of the modeled dispersion curve (dotted line: initial model; continuous line: end model). Horizontal axis: frequency Hz, vertical axis: v_s.*
***blue**: 10-layer-model (dotted: initial model, continuous line: final model). Horizontal axis: depth, vertical axis: phase velocity resp. v_S).*
1st row: left: station 25 @ PLUS direction; right: station 30 @ MINUS direction
2nd row: left: station 31 @ PLUS direction; right: station 36 @ MINUS direction
3rd row: left: station 39 @ PLUS direction; right: station 42 @ MINUS direction
4th row: left: station 47 @ PLUS direction; right: station 48 @ MINUS direction

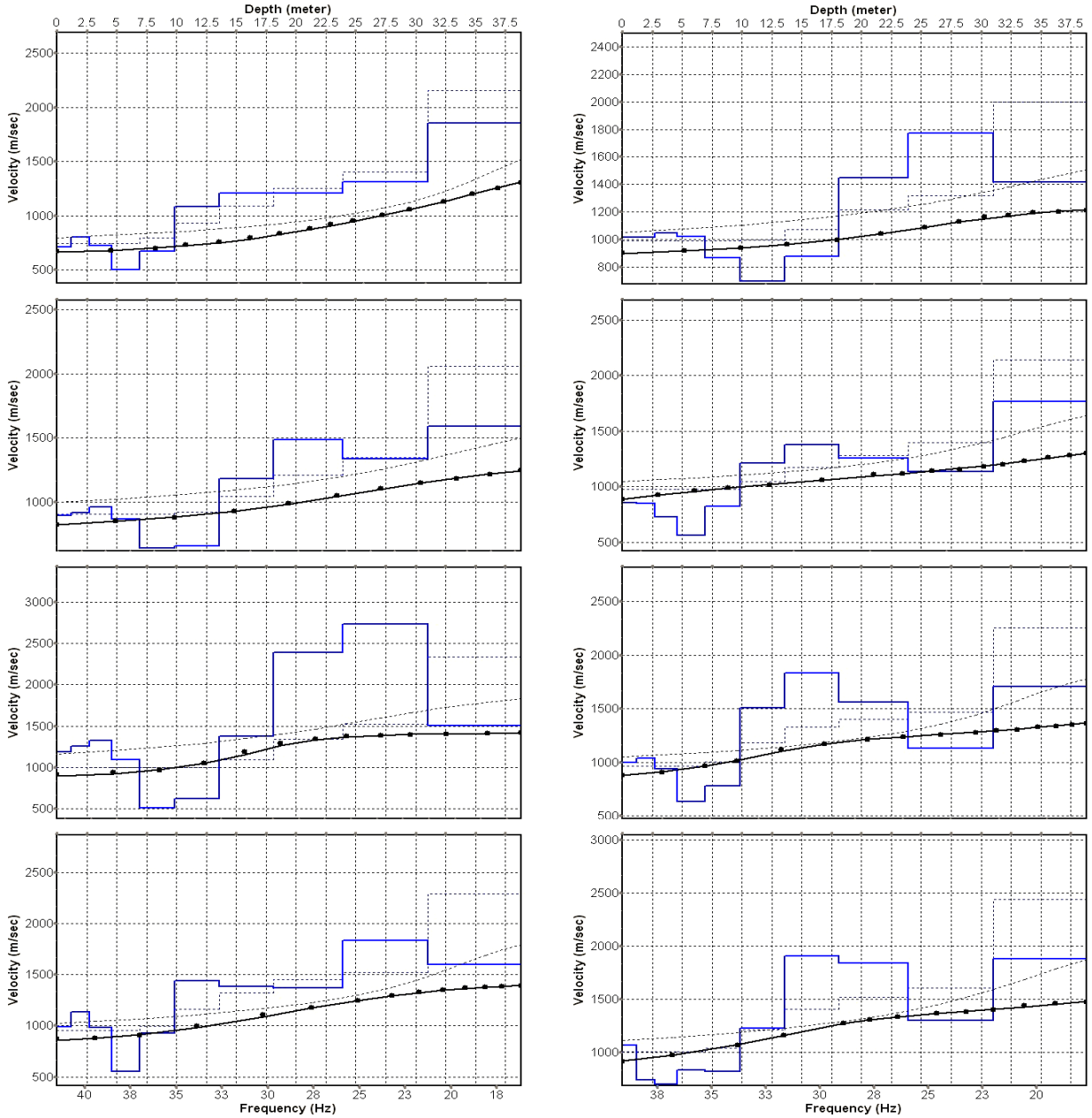

Fig. 3.3e: Inversion results of dispersion curves of dataset at line 09SN_06BRANT-M2.
***brown**: Inversion of dispersion curve (dots) resp. of the modeled dispersion curve (dotted line: initial model; continuous line: end model). Horizontal axis: frequency Hz, vertical axis: v_s.*
***blue**: 10-layer-model (dotted: initial model, continuous line: final model). Horizontal axis: depth, vertical axis: phase velocity resp. v_S).*
1st row: left: station 25 @ PLUS direction; right: station 27 @ MINUS direction
2nd row: left: station 39 @ PLUS direction; right: station 42 @ MINUS direction
3rd row: left: station 54 @ PLUS direction; right: station 60 @ MINUS direction
4th row: left: station 75 @ PLUS direction; right: station 72 @ MINUS direction

Dispersion analyses of records with longer receiver arrays should – by theory – increase the investigation depth. At BRANT, with both lines and both directions, MASW processing with the maximal array length of 96 m doesn't improve the results (Fig. 3.3f and 3.3g).

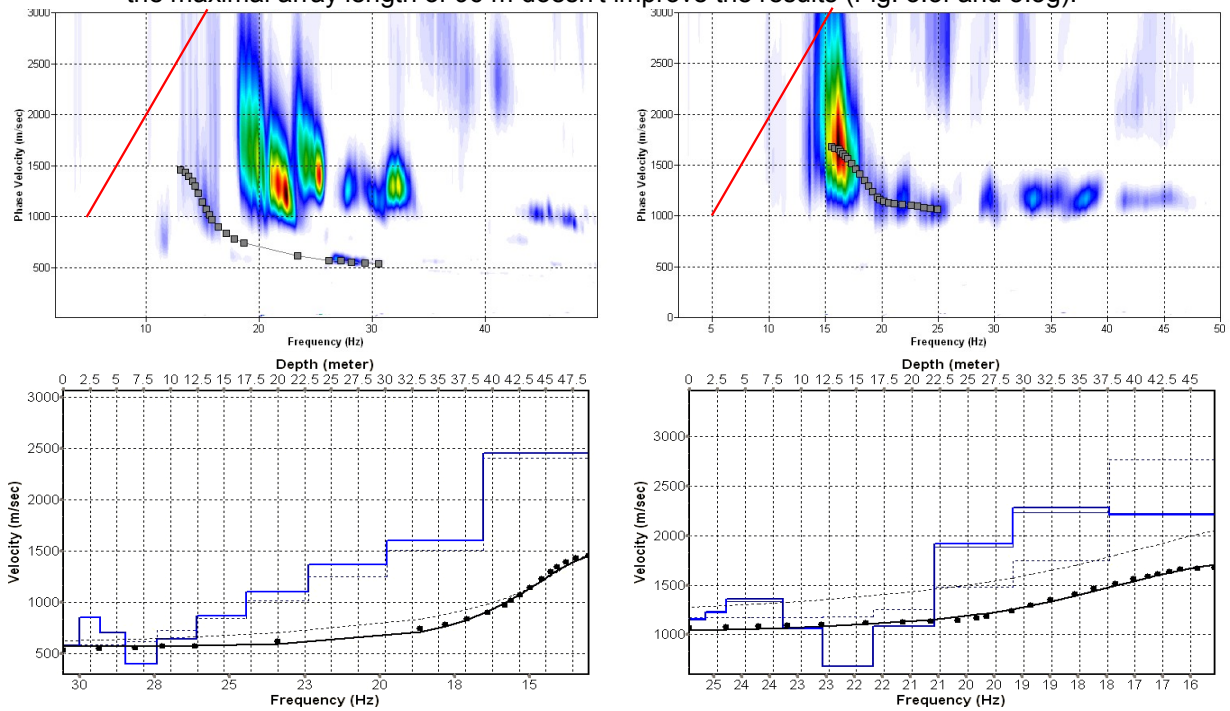

Fig. 3.3f: Top: dispersion images of over-all arrays (10...106 m offset) of line 09SN_06BRANT-M1 in PLUS (left) and MINUS (right) direction; dotted fine line: signal-noise ratio for the designated f-v_{ph}-value. Red line: high resolution beam-forming curve for v_{max}.
*Below: The two respective inversion results; **brown**: inversion of dispersion curve; **blue**: 10-layer-model. Horizontal axis: depth, vertical axis: phase velocity resp. v_s.*

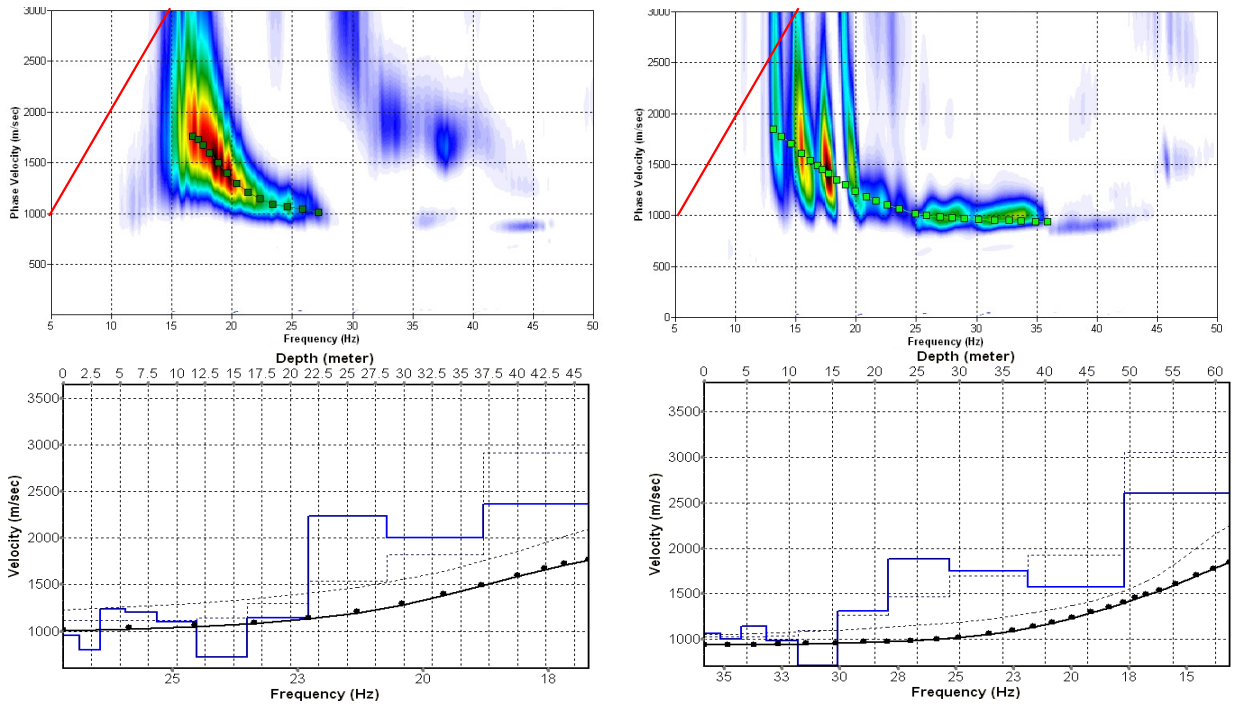

Fig. 3.3g: Top: dispersion images of over-all arrays (10...106 m offset) of line 09SN_06BRANT-M2 in PLUS (left) and MINUS (right) direction; dotted fine line: signal-noise ratio for the designated f-v_{ph} – value. Red line: high resolution beam-forming curve for v_{max}.
*Below: The two respective inversion results; **brown**: inversion of dispersion curve; **blue**: 10-layer-model. Horizontal axis: depth, vertical axis: phase velocity resp. v_s.*

3.3.5 Gridding and plotting of 2D v_s-velocity field

By assembling the 1D v_s - depth functions of all stations the final 2D v_s-field is derived using a Kriging gridding procedure as portrayed in Fig. 3.3h and 3.3i below:

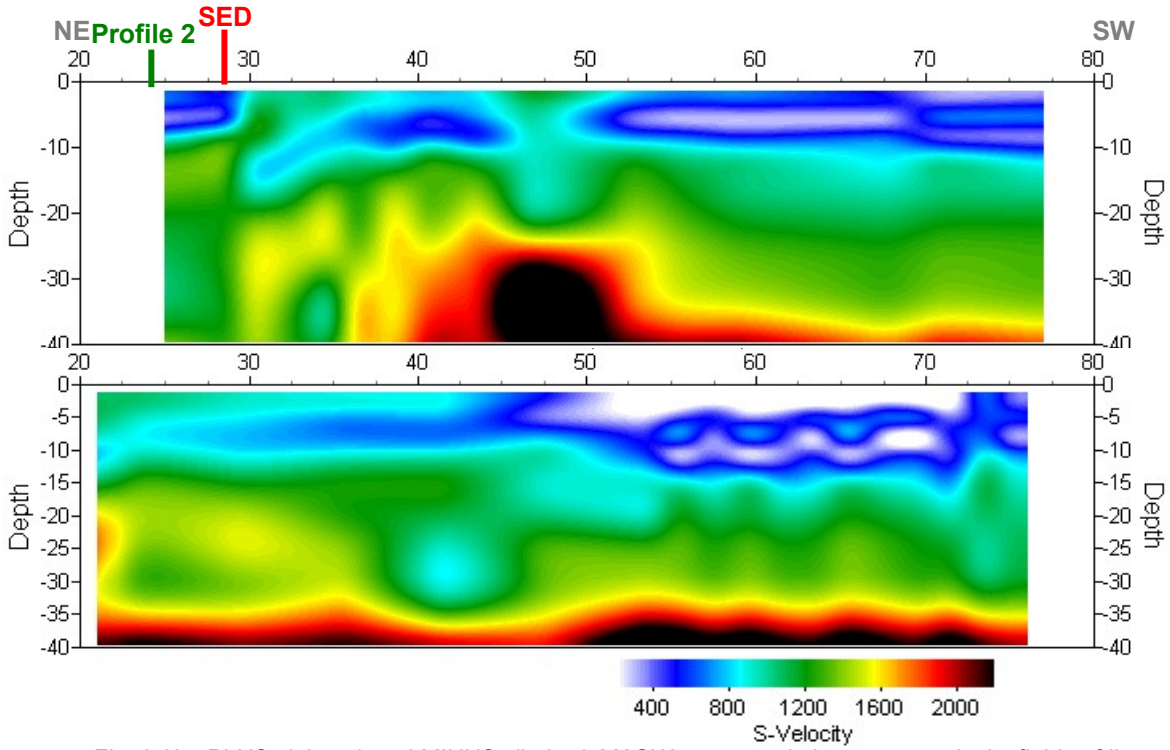

Fig. 3.3h: PLUS- (above) and MINUS- (below)-MASW-processed shear wave velocity fields of line 09SN_06BRANT-M1. Station spacing is 1 m.

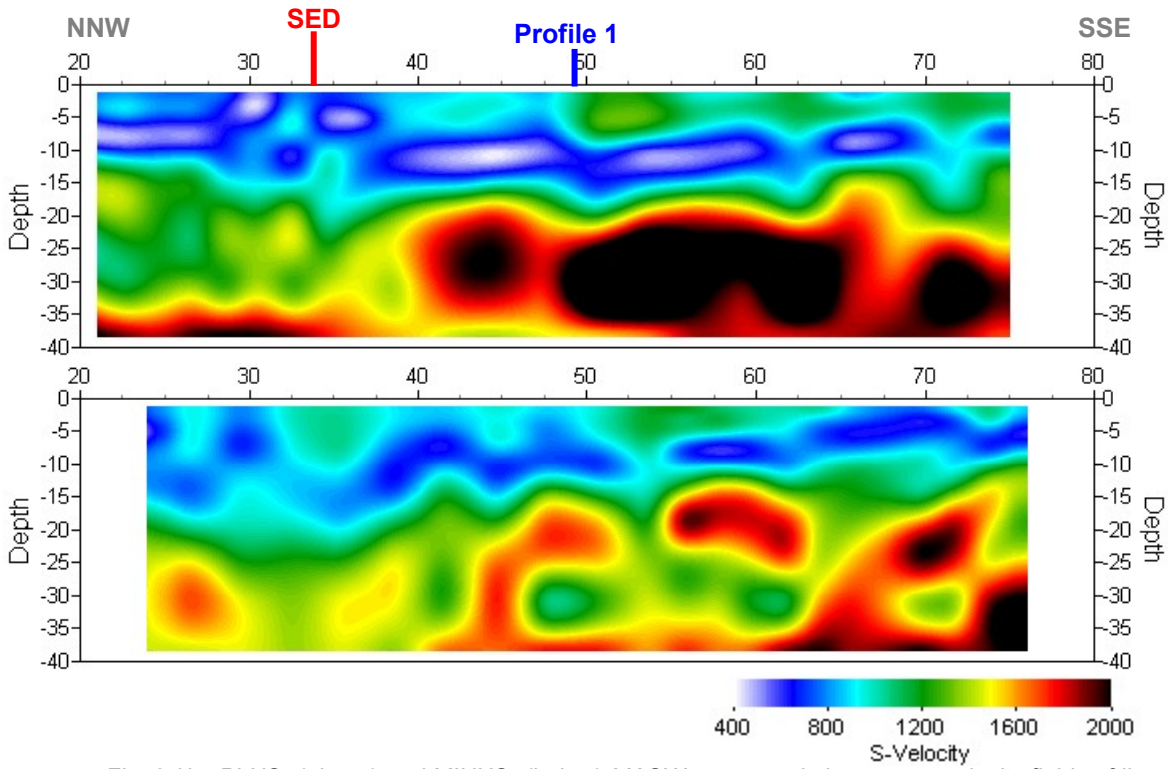

Fig. 3.3i: PLUS- (above) and MINUS- (below)-MASW-processed shear wave velocity fields of line 09SN_06BRANT-M2. Station spacing is 1 m.

3.3.6 Calculation of the average shear wave velocity

In order to calculate a representative shear wave velocity-depth function of line 09SN_06BRANT-M1 at the SED station, all computed 1D-v_S-depth functions between seismic profile station no. 25 and 50 are averaged (non-weighted mean values). The v_S-depth-function is shown in Tab. 3.3a.

Depth [m]	Vs- [m/s]	Vs- [m/s]	Vs [m/s]
0.0	922	1049	986
1.3	931	1103	1017
2.9	810	1005	907
4.9	833	938	885
7.4	1002	883	943
10.6	1211	978	1094
14.5	1294	1301	1298
19.4	1383	1613	1498
25.6	1406	1625	1516
33.2	2097	1518	1808

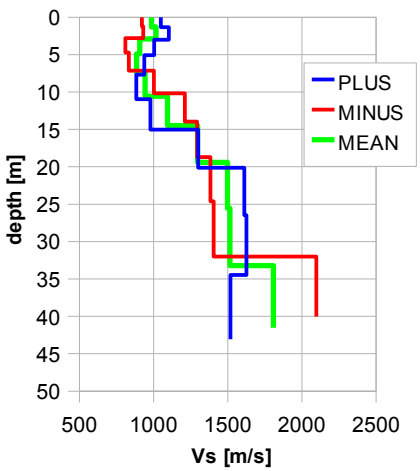

Tab. 3.3a: Averaged vs - depth function of line 09SN_06BRANT-M1 at the SED station. Blue line: MASW-'PLUS' processing, red line: MASW-'MINUS' processing; green line: average of PLUS- and MINUS-functions.

In order to calculate an representative shear wave velocity-depth function of line 09SN_06BRANT-M2 at the SED station, all computed 1D-v_S-depth functions are averaged (non-weighted mean values). The resulting v_S-depth-function is shown in Tab. 3.3b.

Depth [m]	Vs- [m/s]	Vs+ [m/s]	Vs [m/s]
0.0	966	872	919
1.2	909	934	922
2.7	836	901	869
4.6	787	753	770
6.9	872	676	774
9.9	1097	901	999
13.5	1373	1262	1318
18.1	1496	1610	1553
23.9	1477	1749	1613
31.1	1743	1756	1750

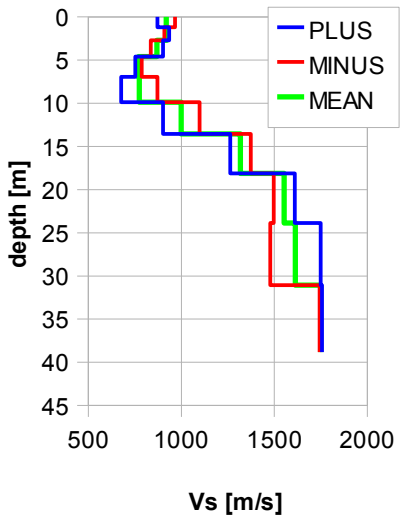

Tab. 3.3b: Averaged v_S - depth function of line 09SN_06BRANT-M2 at the SED station. Blue line: MASW-'PLUS' processing, red line: MASW-'MINUS' processing; green line: average of PLUS- and MINUS-functions.

The inversion of the four 100 m-array dispersion curves data (10 to 106 m offset, see Fig. 3.3f and 3.3g) are given in Tab. 3.3c. These values are complemented with the values derived of the 40 m-arrays analyses (Tab. 3.3a and 3.3b).

100 m array								40 m array			
depth	m1+	m1-	m2+	m2-	m1	m2	m	depth	m1	m2	m
1.6	582	1157	957	1061	870	1009	899	0.0	986	919	952
3.6	857	1233	800	1006	1045	903	964	1.2	1017	922	969
6.0	703	1356	1237	1146	1029	1191	1099	2.8	907	869	888
9.1	398	1360	1206	985	879	1095	988	4.7	885	770	828
13.0	646	1072	1100	713	859	907	939	7.2	943	774	858
17.8	868	679	722	1313	774	1017	756	10.2	1094	999	1047
23.9	1106	1088	1142	1884	1097	1513	1112	14.0	1298	1318	1308
31.4	1367	1916	2233	1753	1642	1993	1839	18.8	1498	1553	1525
40.8	1605	2278	2001	1572	1941	1787	1961	24.7	1516	1613	1564
51.0	2453	2210	2365	2605	2331	2485	2342	32.1	1808	1750	1779

Tab. 3.3c: v_S-depth values of the four MASW-derived dispersion curves of both seismic line 09SN_06BRANT-M1 and 09SN_06BRANT-M2 using 100 m-arrays. The dispersion curves are shown in Fig. 3.3f and Fig 3.3g.

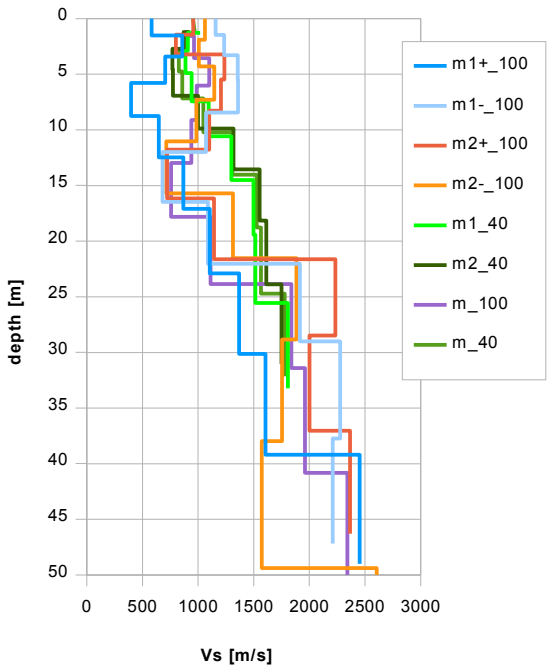

Fig. 3.3j: Comparison of the ensemble of inversion results of both lines 09SN_06BRANT-M1 and -M2, either using the 40 m- and the 100 m-arrays.
blue lines: analyses of records of line 09SN_06BRANT-M1
red lines: analyses of records of line 09SN_06BRANT-M2
magenta line: mean of both 100 m-array records analyses in MINUS and PLUS direction.
green lines: v_S-values of analyses of 40 m-array records.

3.3.7 Calculation of the shear wave velocity scalars $v_{s,5}$, $v_{s,10}$, ...

The parameters $v_{s,5}$, $v_{s,10}$, $v_{s,20}$, $v_{s,30}$, $v_{s,40}$, $v_{s,50}$ represent the average shear wave velocities in the depth interval between the surface and the respective depth levels and are determined from the formula

$$v_{s,n} = \frac{\sum_{i=1}^{n} d_i}{\sum_{i=1}^{n} d_i / v_{si}}$$

with:

d_i = thickness of layer i

v_{si} = corresponding shear-wave velocity.

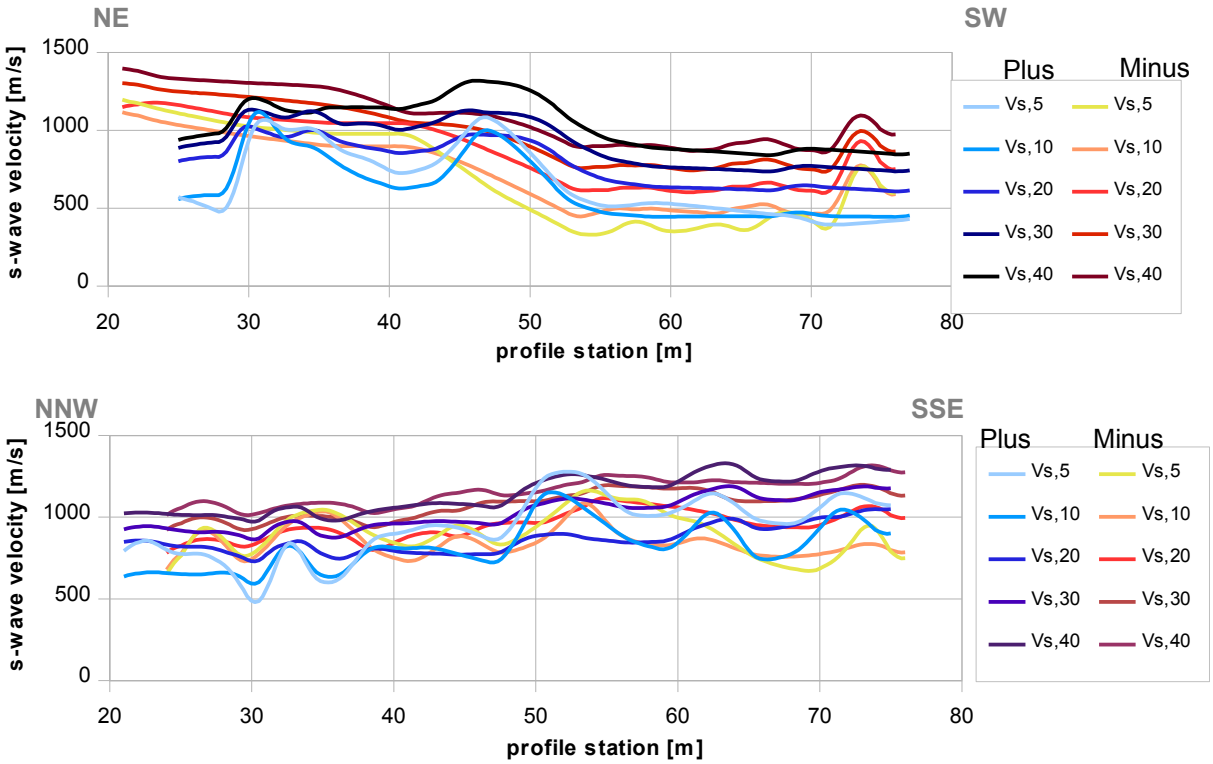

Fig. 3.3k: Graphs of the averaged $v_{s,5}$...-values along the line 09SN_06BRANT-M1 (top) and -M2 (bottom) for the PLUS- (blue lines) and MINUS- (red lines) directions.

The average values of the s-wave velocity model $v_{s,5}$, $v_{s,10}$, $v_{s,20}$, $v_{s,30}$, $v_{s,40}$, $v_{s,50}$, $v_{s,100}$ (= average shear wave velocity from the surface to depths of 5 m, …until 100 m) on the line segment nearest to the SED station (Tab. 3.3d) are summarized below:

	Vs,5	Vs,10	Vs,20	Vs,30	Vs,40	Vs,50
MINUS	896	866	1010	1106	1199	n/a
PLUS	843	793	922	1054	1161	n/a
MEAN	870	830	966	1080	1180	n/a

	Vs,5	Vs,10	Vs,20	Vs,30	Vs,40	Vs,50
MINUS	904	849	953	1077	1158	n/a
PLUS	939	823	863	1026	1141	n/a
MEAN	921	836	908	1051	1150	n/a

Tab. 3.3d: The average shear wave velocities within the depth intervals from surface down to 5 m, etc.… to 50 m, calculated for the line segment with a subjectively most similar geology to the SED station (profile station 45 to 65 for line 09SN_06BRANT-M1, above; profile stations 30 to 55 for line 09SN_06BRANT-M2, below).

3.4 Hybrid Seismic Data Processing

3.4.1 p-wave *Reflection* Seismic Processing Sequence

A) Data conditioning

A1 Reformatting and quality verification of field data
A2 Recording geometry assignment
A3 Data editing (suppression of bad / dead traces, etc.)
A4 Preliminary analysis of refraction velocities

B Filtering and deconvolution

B1 Analytical muting of refraction arrivals
B2 Amplitude recovery / amplitude equalization in time and frequency domains
B3 Predictive deconvolution parameter tests / application
B4 Determination of band limiting corner frequencies / application
B5 Optional 2-D filtering

C) Velocity analysis and stack

C1 Common Depth Point (CDP) sort
C2 Semblance velocity analysis using supergathers of 3 - 5 CDP's
C3 Optional dip move-out correction
C4 Normal Move-Out (NMO) correction and application of stretch mute
C5 Band-pass filtering
C6 CDP stack
C7 Optional coherency filtering

D) Time-depth conversion

D1 Optional spiking deconvolution
D2 Band-pass filtering
D3 Depth conversion
D4 Final display of seismic depth section with inversed polarity (non-SEG-convention)

3.4.2 The presentation of reflection seismic data

The data in a reflection seismic section are presented as an assembly of individual seismic signals at regular intervals along a seismic profile. The simplest way of representing the signals are single wiggle lines (first to the left in the illustration below). A more capturing presentation is the variable area form (second to the left). Combining these two modes results in the var-wiggle mode. Another method of data visualization is the variable density mode (second from the right).

The compressional phase of seismic signals is defined in this report as the onset of the positive amplitude excursion in black (Fig. 3.4a). Since the source signal is produced by an explosion or by an impact at the surface, the signal starts off with a compression of the ground particles. Thus the arrivals of reflection events are defined by the compressional phase.

In rare situations of velocity inversions, cases in which formation velocities are lower than in the layers above, polarity reversals of the reflected signals occur. The beginning of the reflection event would then be characterized by a dilatational phase, represented in this report as a negative amplitude excursion, i.e. in white.

The final p-wave seismic depth sections are displayed in Fig. 3.4b and 3.4c, the hybrid sections in Fig. 3.4j and -k further below.

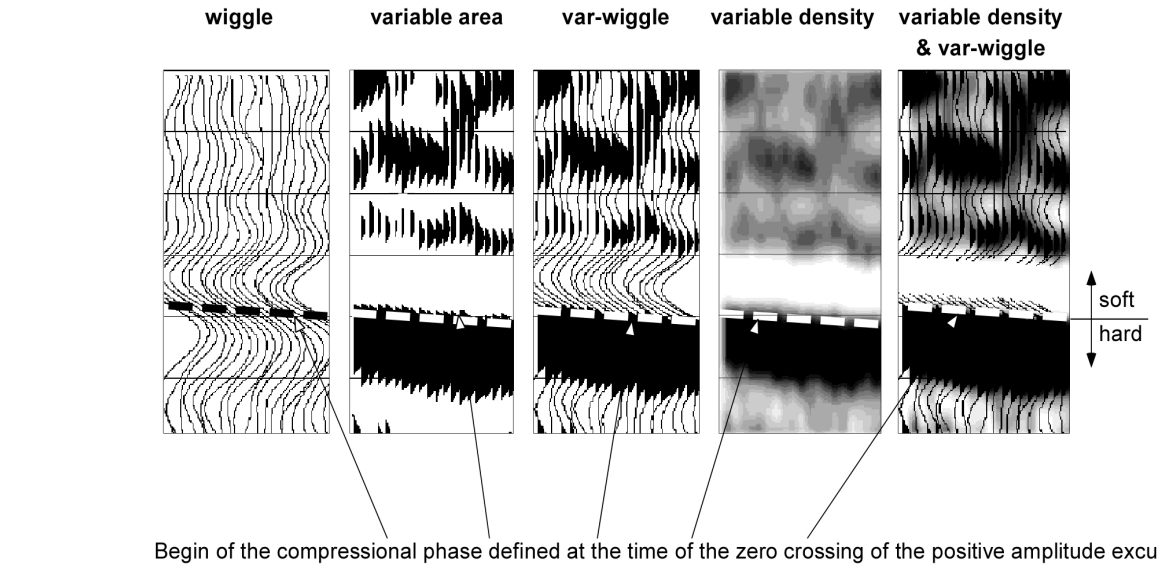

Fig. 3.4a Representation of reflection seismic data and the definition of a reflection event.

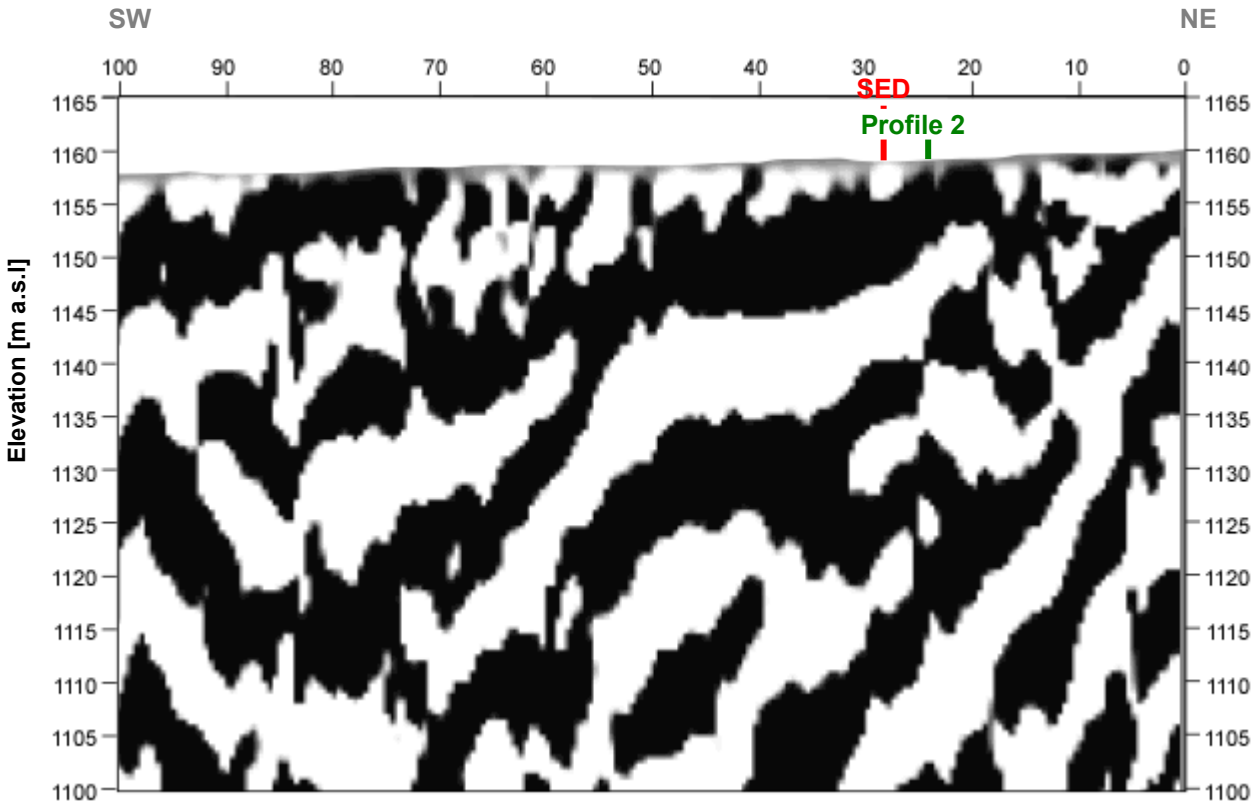

Fig. 3.4b: Seismic depth section of seismic line 09SN_06BRANT-P1 with variable density mode presentation. Vertical axis: elevation [m a.s.l.], horizontal axis: profile meter; no vertical exaggeration. The station spacing is 1 m.

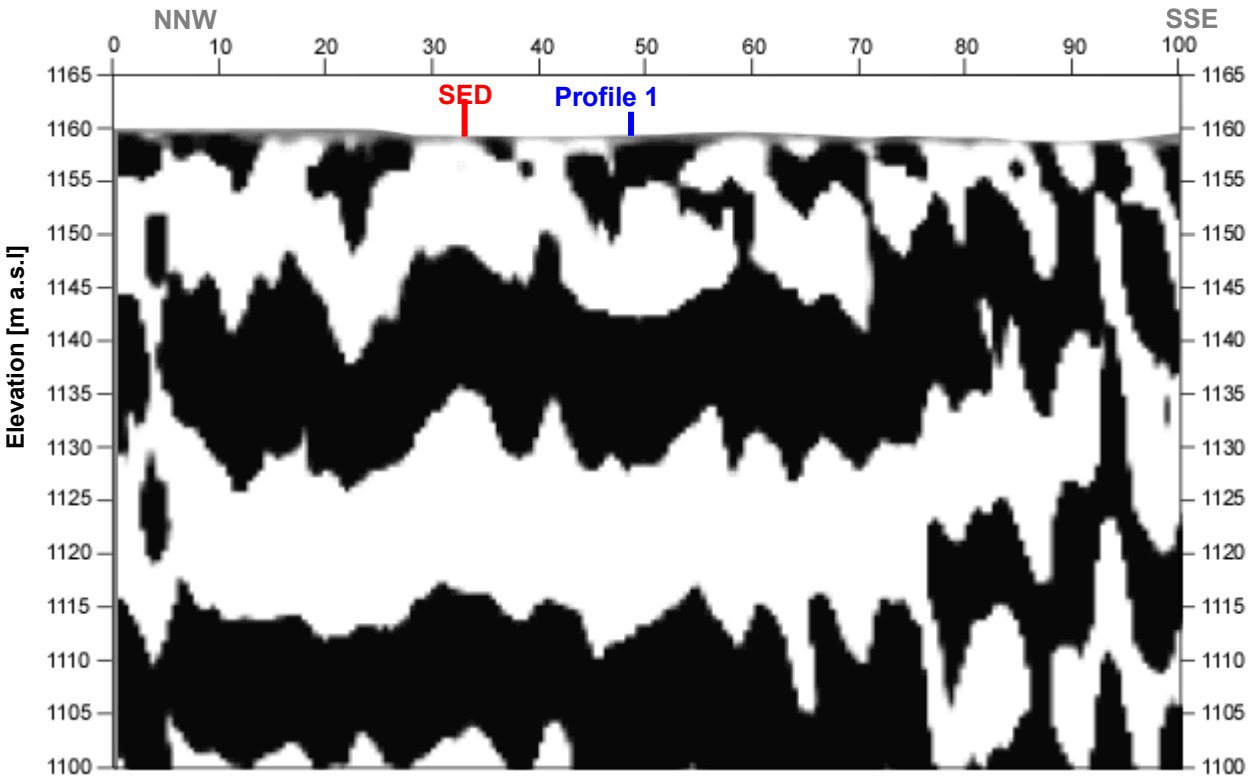

Fig. 3.4c: Seismic depth section of seismic line 09SN_106BRANT-P1 with variable density mode presentation. Vertical axis: elevation [m a.s.l.], horizontal axis: profile meter; no vertical exaggeration. The station spacing is 1 m.

3.4.3 p-wave refraction tomography processing

The seismic p-wave refraction processing steps are analogous to those described in paragraph 3.2. For a detailed method statement and a description of the processing steps please refer to the summary report. The Figs. 3.4d to 3.4i and Tab. 3.4a illustrate the intermediate processing steps and the final result.

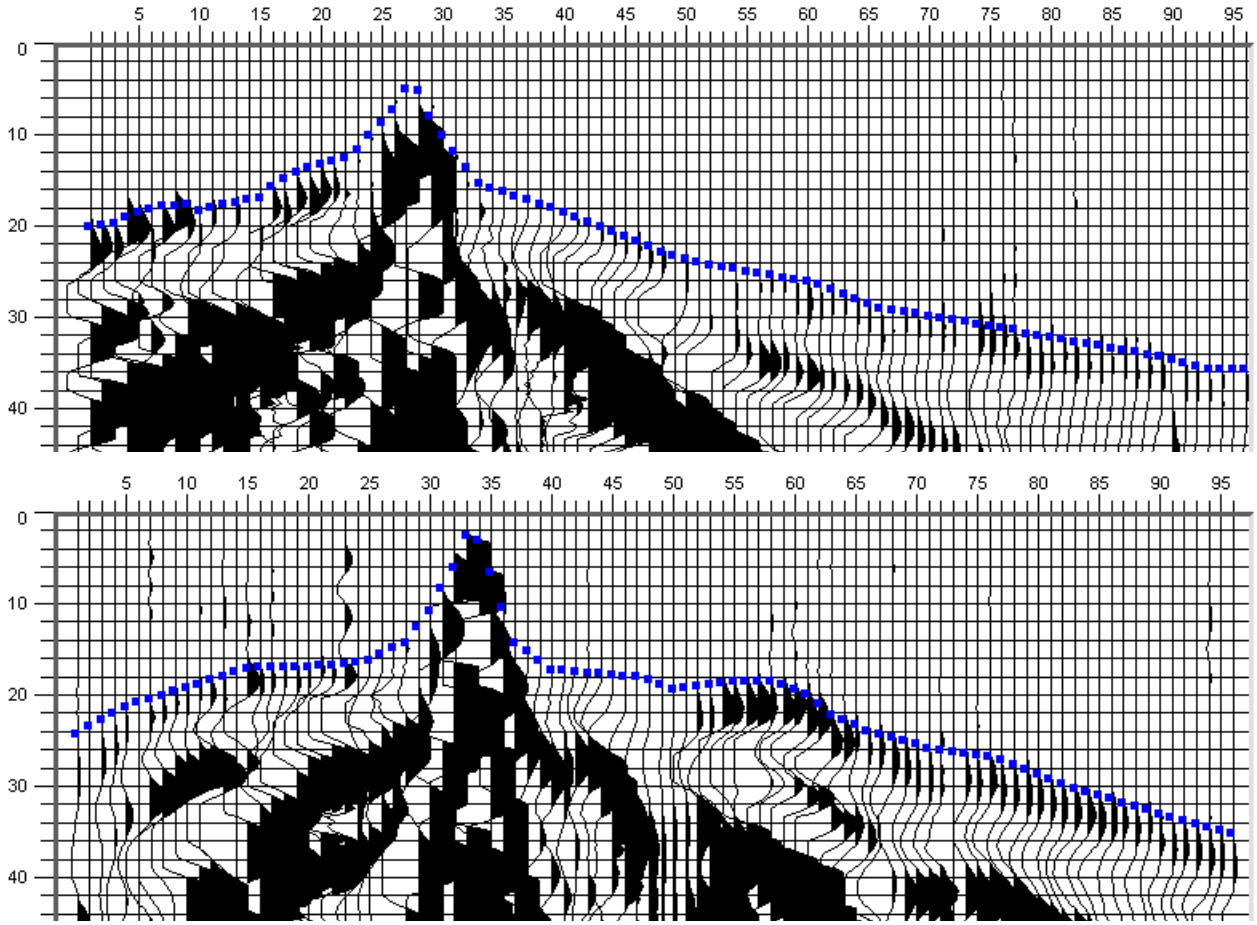

Fig. 3.4d: p-wave records of 09SN_06BRANT-P1 (top) and -P2 (bottom) with positive amplitude excursions in black. Blue squares mark the manually picked first break arrival times. Vertical axis: travel time in ms, horizontal axis: station numbers spaced at 1 m.

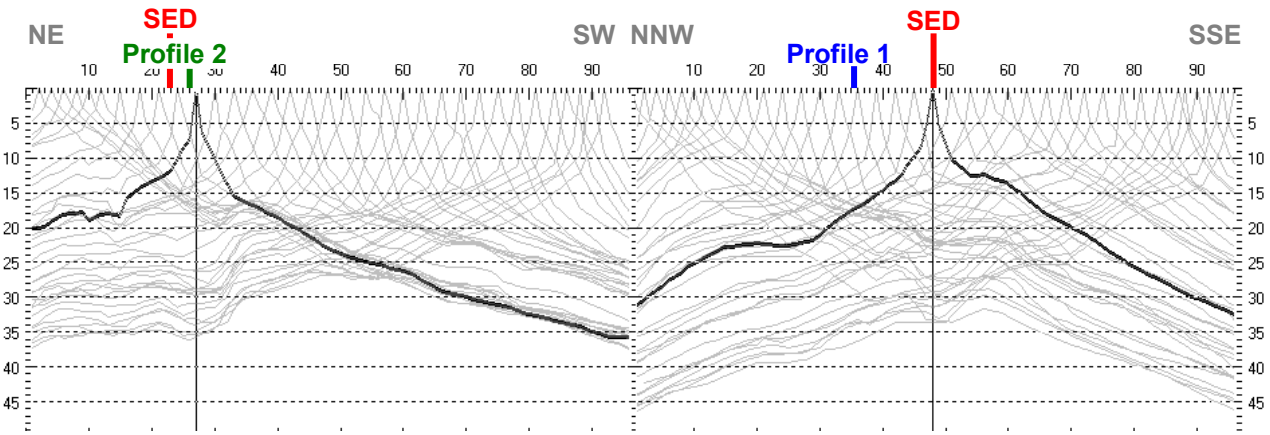

Fig. 3.4e: Travel time curves of p-wave arrival time picks of line 09SN_06BRANT-P1 (left) and -P2 (right). Vertical axes: travel time [ms], horizontal axes: station number (= profile meter).

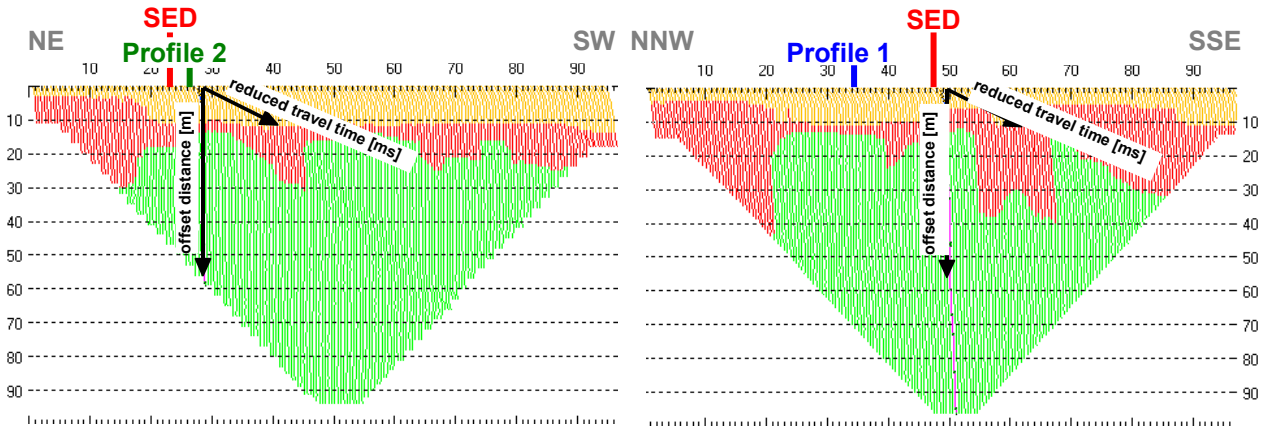

Fig. 3.4f: 3-dimensional distance-travel time diagrams at the mid-points between source points and receiver stations are instrumental when using the analytical CMP derivation of the initial velocity field. The horizontal axes are along the CMP positions and the travel time respectively, the vertical axis denotes the offset distance between source and receiver positions.

Depth [m]	Vp [m/s]
0.0	281
0.2	348
0.5	433
1.2	625
1.7	772
2.4	967
3.2	1231
4.4	1693
5.9	2428
8.0	3274
10.5	3358
13.9	3956
18.3	4988
23.9	5343
31.4	5494

Depth [m]	Vp [m/s]
0.0	283
0.2	345
0.5	449
0.8	572
1.2	711
1.9	1009
2.5	1299
3.6	1662
4.9	2109
6.4	2578
8.6	2870
11.5	3016
15.1	3174
19.8	3874
25.9	4269
34.1	5042

Tab. 3.4a: Initial 1D p-wave velocity model derived from real data (left: 09SN_06BRANT-P1; right: -P2).

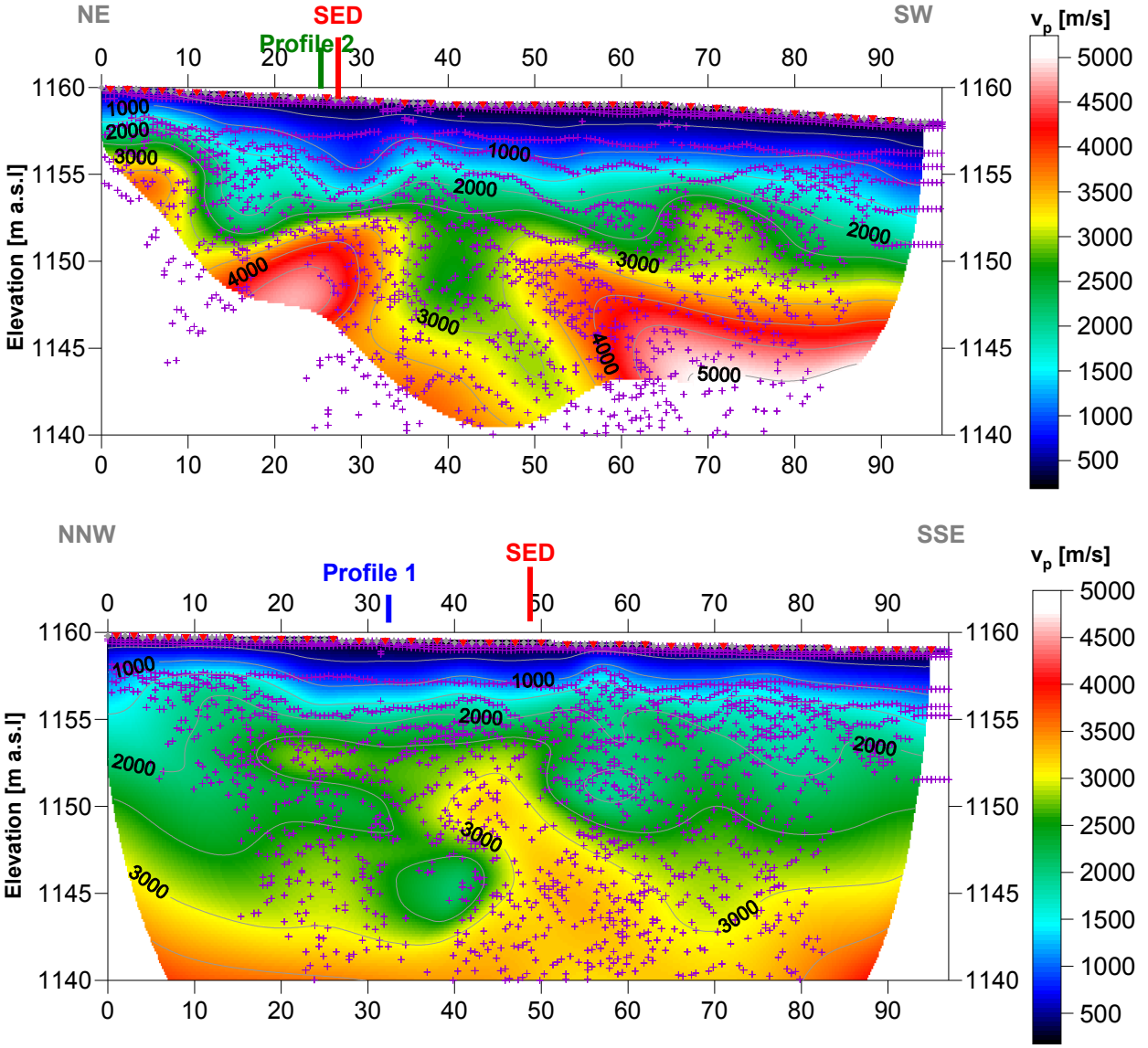

Fig. 3.4g: Compressional wave velocity field image along the seismic profiles 09SN-06BRANT-P1 (top) and -P2 (bottom). Red/white colors indicate solid rock, blue/black colors unconsolidated sediments and soil. Vertical axis: elevation [m a.s.l]; horizontal axis: profile meter; color scale: v_s [m/s]; vertical exaggeration: 2:1; gray squares: receiver stations; red triangles: shot positions; magenta crosses: positions of determined velocity values.

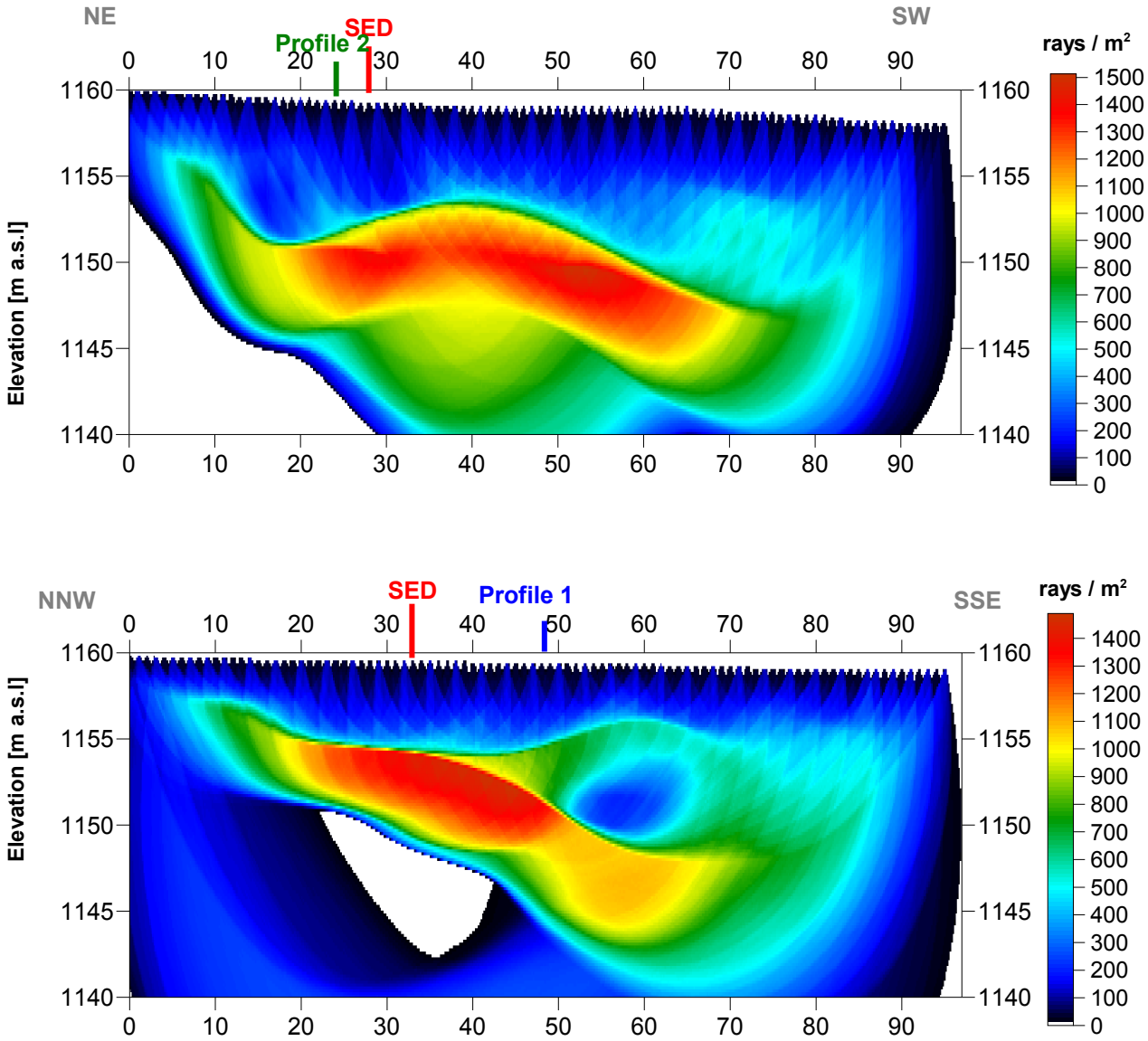

Fig. 3.4h Compressional wave subsurface ray path density along the seismic profiles 09SN_06BRANT-P1 (top) and -P2 (bottom). Red/white colors indicate high velocity contrast between two layers, blue/black colors low coverage areas. Vertical axis: elevation [m a.s.l]; horizontal axis: profile meter; color scale: ray paths per m2; vertical exaggeration: 2:1.

Depth [m]	Vp [m/s]
0.0	283
1.2	560
2.2	865
3.2	1166
4.2	1527
5.3	1976
6.3	2498
7.3	2970
8.3	3248
9.3	3357
10.4	3395
11.4	3392
12.4	3314
13.4	3233
14.4	3262
15.4	3323
16.5	3372
17.5	3439
18.5	3544

Depth [m]	Vp [m/s]
0.0	276
1.7	931
3.4	1627
5.1	2075
6.8	2321
8.5	2381
10.2	2562
11.9	2727
13.6	2827
15.3	2967
16.9	3162
18.6	3345
20.3	3501
22.0	3642
23.7	3766
25.4	3848
27.1	3869
28.8	3701
30.5	3632

Tab. 3.4b: Final 1D p-wave velocity model derived from real data at positions most similar to the geological setting at SED station between profile meters 24 and 55 at line 09SN_06BRANT-P1 (left) resp. over all at line 09SN_06BRANT-P2 (right).

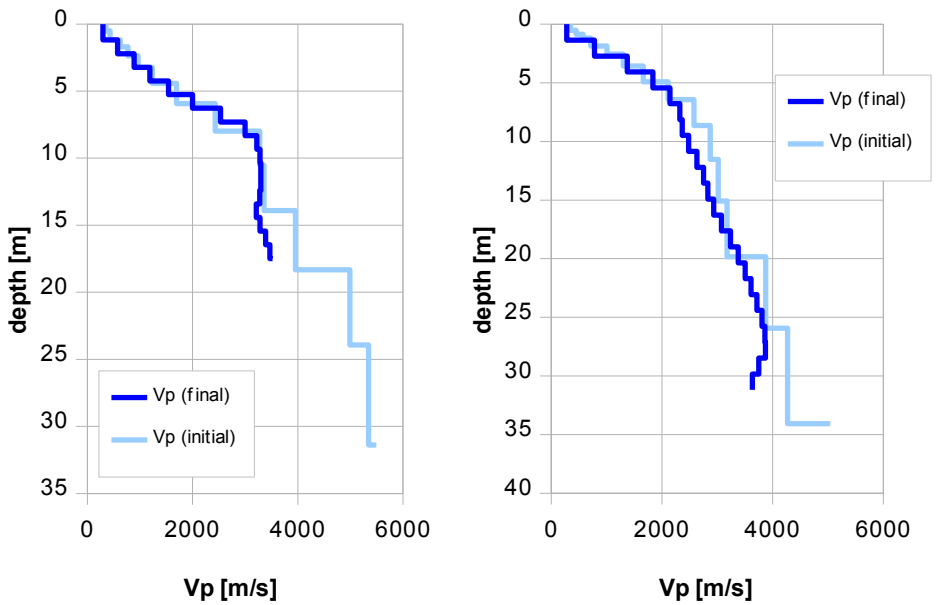

Fig. 3.4i: Final 1D p-wave velocity model derived from real data at a position most similar to the geological setting at the SED station between profile meters 25 and 50 at line 09SN_06BRANT-P1 (left) resp. over all at line -P2 (right). Initial 1D p-wave velocity model values are given in Tab. 3.4a.

3.4.4 Representation of the hybrid seismic section

The hybrid seismic section is the reflection seismic section with the superimposed p-wave velocity field. It portrays the geological structures and the p-wave velocity field, the latter being indicative for the rock rigidity. The uninterpreted hybrid seismic section are given below.

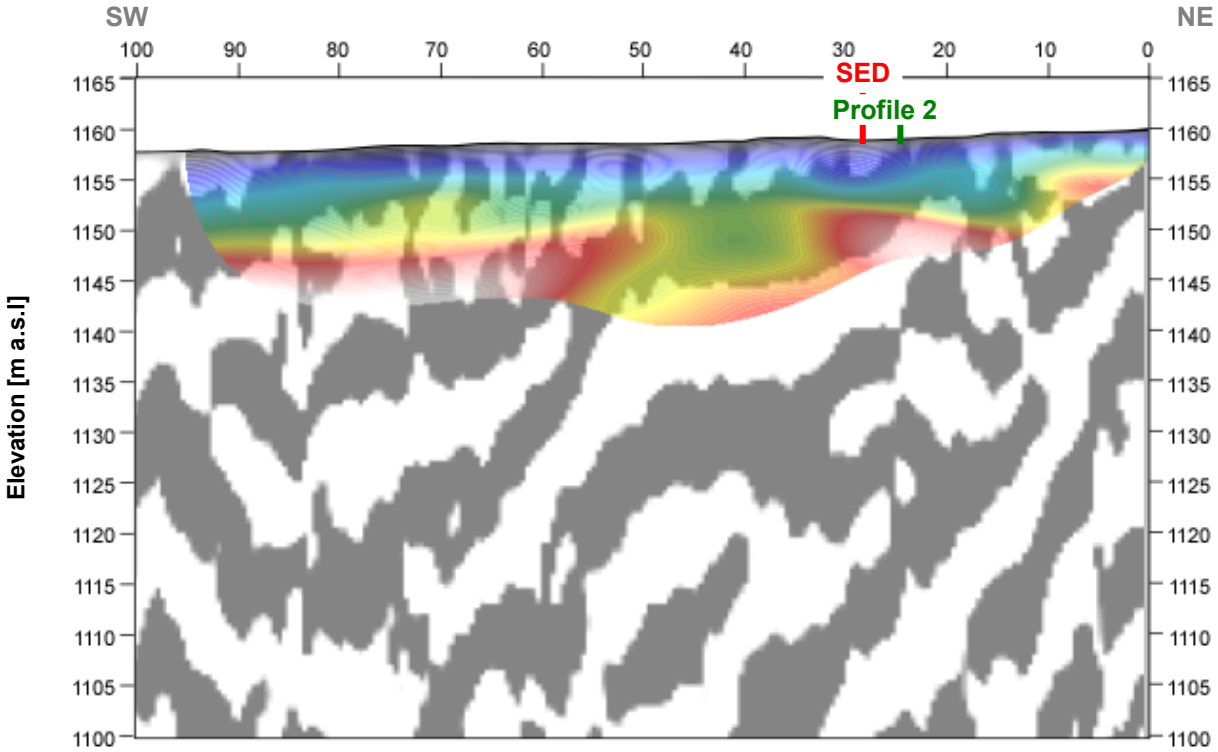

Fig. 3.4j Uninterpreted hybrid seismic section 09SN_06BRANT-P1: superimposed onto the seismic reflection section is the color encoded p-velocity field derived by refraction tomography (no vertical exaggeration).

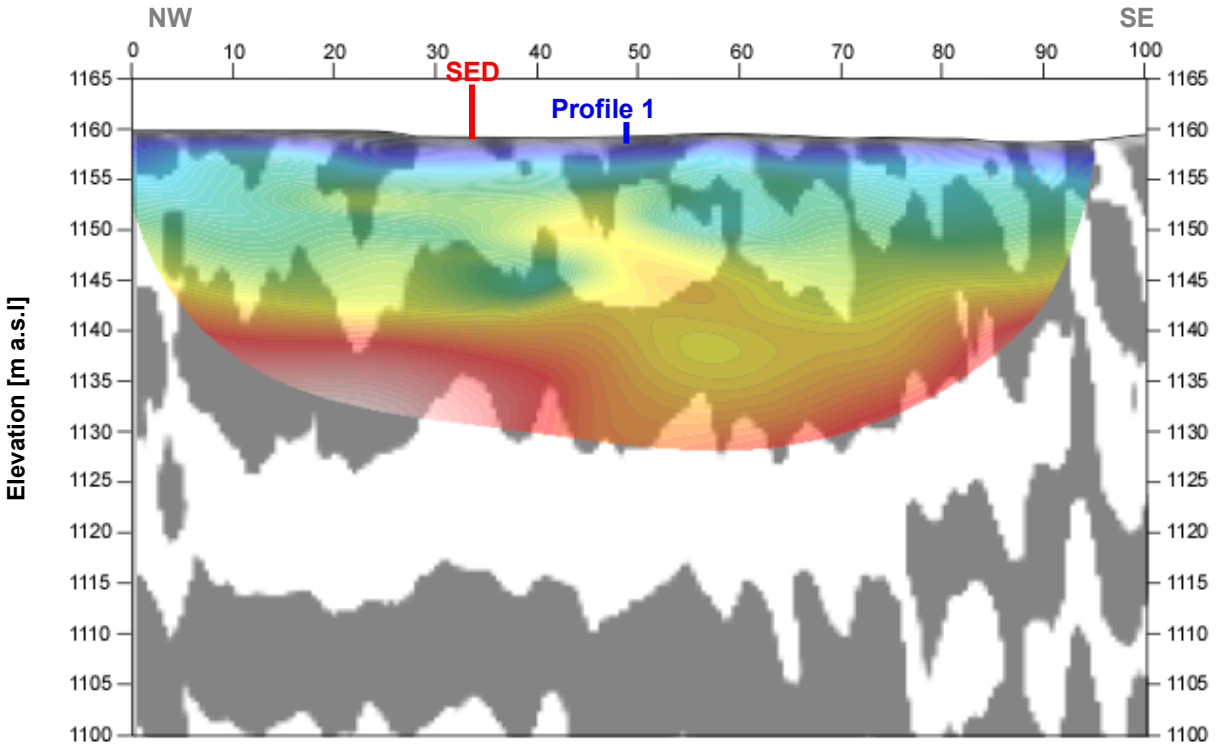

Fig. 3.4k Uninterpreted hybrid seismic section 09SN_06BRANT-P2: superimposed onto the seismic reflection section is the color encoded p-velocity field derived by refraction tomography (no vertical exaggeration).

4 DISCUSSION OF THE RESULTS

4.1 Summary and Validation of the Results

Compressional and shear wave velocity data from refraction seismic surveys both p-wave and s-wave and also the MASW survey data of profiles 09SN_06BRANT-1 and 09SN_06BRANT-2 are shown in Tab. 4.1 for the uppermost 30 m. The calculated shear wave velocity $v_{s(calc)}$ in Tab. 4.1 is derived by using a theoretical v_p/v_s-ratio of $\sqrt{3}$.

Z	Vp1	Vp2	Vs1	Vs1	Vs2	Vs2	Vs1	Vs2
[m]	meas	meas	meas	calc	meas	calc	MASW	MASW
0	293	276	136	169	191	159	986	919
1					318		1017	922
2	574		406	331	507			
3	886	778		512		449	907	869
4	1185	1371	810	684	711	792		
5	1543	1835		891	915	1059	885	770
6	1999		1174	1154	1044			
7	2528	2142		1460	1013	1237	943	774
8	2996	2321		1730		1340		
9	3221	2365	1582	1860	978	1365		
10	3281			1894	1072			999
11	3297	2481	1890	1904	1218	1432	1094	
12	3297	2631		1903	1324	1519		
13	3277		1846	1892				
14	3210	2754		1853	1386	1590		1318
15	3282	2827	1769	1895	1522	1632	1298	
16	3385	2933		1954	1699	1694		
17	3467		1800	2002	2020			
18		3076			2503	1776		1553
19		3236	1786			1868	1498	
20		3377			2873	1950		
21			1849					
22		3501				2021		
23		3608	1993			2083		
24		3714				2144		1613
25								
26		3808	2143			2199	1516	
27		3857				2227		
28		3869	2274			2234		
29								
30		3747	2373			2163		

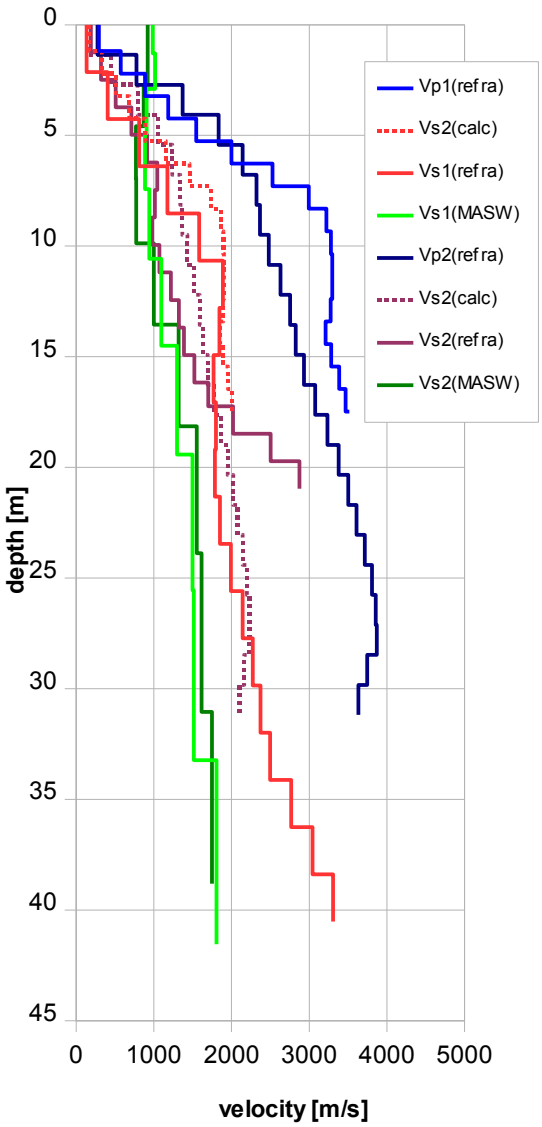

Tab. 4.1: Shear and compressional wave velocity model determined at the SED station BRANT.

Fig. 4.1: Graphic display of shear (continuous lines) and compressional (dotted lines) wave velocities determined at the SED station. In green colors values of MASW derivation, in blue compressional and in red shear wave velocity values from refraction tomography.

4.2 Validation of the methods and their results

Due to methodological differences, v_s velocities derived by MASW analysis and by the refraction tomography technique may differ considerably. This is because MASW analysis cannot image small rock/soil inhomogeneities as a dispersion image with an array length of i.e. 40-m only yields one single v_s-value at each depth. On the other hand, refraction diving wave tomography results produce v_s-sections with a high lateral resolution, but fail to provide information at greater depths.

4.3 Error Estimates

The error estimates given in Tab. 4.3 below are relevant only in the context of this survey.

Surveying method	Type of result	Error estimate
v_s – refraction tomography	v_s – velocity field image	15%**
MASW only "+" or only "-" values*	v_s – velocity field image	15%
MASW (mean of "+" & "-" values)*	v_s – velocity field image	10%
v_p – refraction tomography	v_p – velocity field image	10%
Reflection seismic surveying	Image of subsurface structures	n.a.

** MASW values in the uppermost 4 m are prone to an error of about 30 % (only one direction) resp. 20 % (mean of both directions.*
*** Refraction shear wave data are prone to an error of about 30 % in the lower part of the model.*

Tab. 4.3 Error estimates for the methods applied. Note that higher error estimates are to be taken into account with increasing depths.

The above error estimates are of a qualitative character only. In view of the intense fluctuations to be expected in both the lateral and vertical directions, any attempt to derive a quantitative general error estimate to be valid for the entire survey is to be considered as futile. In particular the topography variations on line 09SN_06BRANT-1 have a certain impact on the quality of dispersion images. Nevertheless, all velocity data coincide well, independently of the methodological differences.

At the SED station BRANT (Les Verrières NE), the refraction velocity images both from shear and compressional wave analysis show coincident structures, in particular on line 09SN_06BRANT-1. The MASW figures are – except in the uppermost 5 m – consistently 10 to 20 % lower than the values obtained from the shear wave diving wave refraction tomography surveys.

4.4 The Geophysical Interpretation

The most conclusive information about the subsurface structures is provided by the results of the hybrid seismic section (v_p-refraction tomography profiling and reflection seismic section) and confirmed by the evaluation results of the v_s-refraction tomography data.

As can be seen from the v_s and v_p refraction tomography sections in Fig. 3.2e/f & Fig. 3.4g/h, the topography of the bedrock surface is imaged in detail on both profiles. The geological interpretation of the seismic events is shown in Fig. 4.2a. The rock surface seems to outcrop to the Northeastern end. To the South, the bedrock surface deepens down 10 m below terrain. Around profile meter 40, a low velocity zone is visible, maybe that is the cave where the

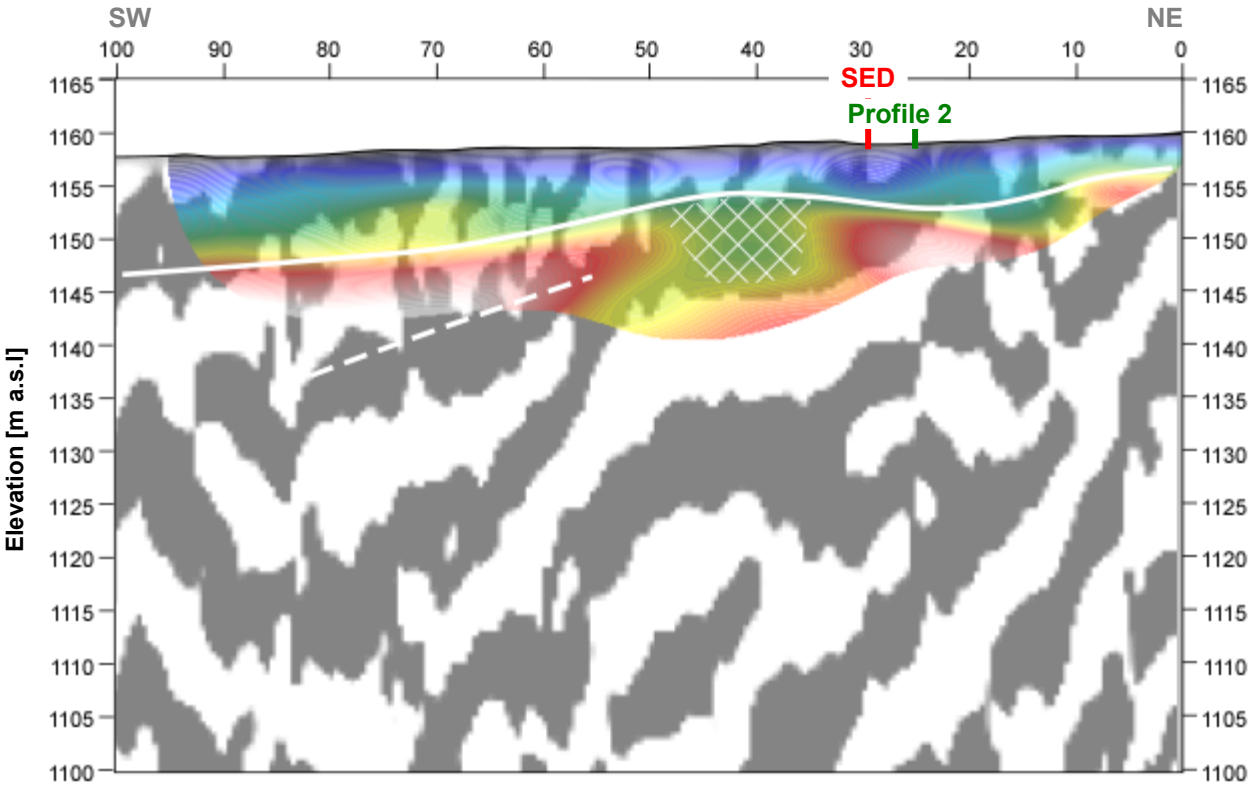

Fig. 4.2a Geophysical interpretation of the hybrid seismic section 09SN_06BRANT-P1. White lines denote layer boundaries, continuous line the bedrock surface. The imaged low velocity zone (white hatched area) corresponds possibly with the cave where the seismological monitoring station is installed in.

The geological interpretation of the seismic events of line 09SN_06BRANT-2 is shown in Fig. 4.2a. As on the first hybrid section, on line 09SN_06BRANT-2 the bedrock topography is imaged in detail all over the profile. In the Northwestern part between profile meter 0 and 40, a velocity inversion is visible. This could be the cave where the earthquake monitoring station is installed in. The layering in the bedrock is sub-horizontal.

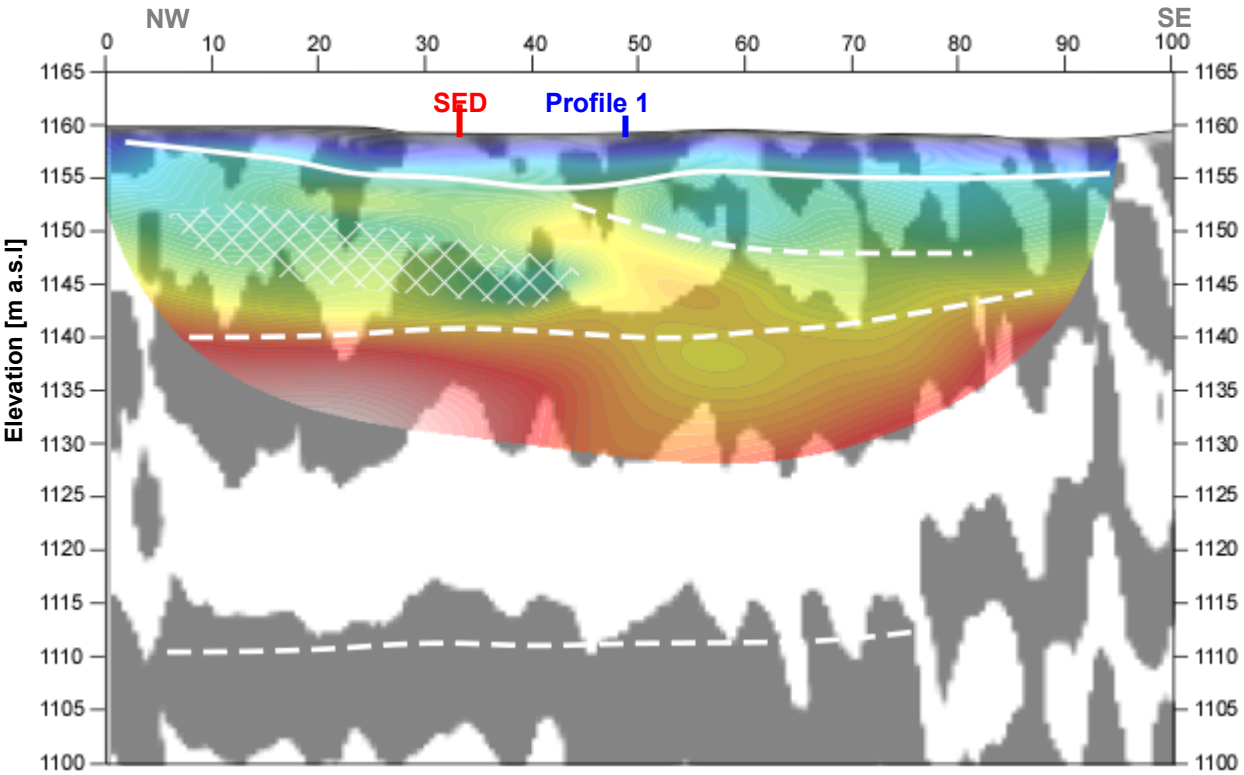

Fig. 4.2b Geophysical interpretation of the hybrid seismic section 09SN_06BRANT-P2. White lines denote layer boundaries, the continuous one marks the bedrock surface. The imaged low velocity zone (white hatched area) corresponds possibly with the cave where the seismological monitoring station is installed in.

5 SUMMARY AND CONCLUSIONS

- In May 2009 a combined seismic s- and p-wave survey was carried out at the SED earthquake monitoring station BRANT near Les Verrières NE.
- The shear wave data have been evaluated by conventional diving wave refraction tomography techniques in order to derive the s-wave velocity field along the seismic line.
- The p-wave data have been processed
  - firstly to derive a 2D s-wave velocity field by using the MASW (**M**ultichannel **A**nalysis of **S**urface **W**aves) technique;
  - and secondly, according to the hybrid seismic data processing scheme for representing the subsurface structures in a combined reflection seismic section with the superimposed p-wave velocity field.
- The shear wave velocity range determined by the MASW method in the uppermost 30 meters spans from values of 770 m/s to 1808 m/s.
- The scalar values derived by the MASW survey at the SED station (seismic line 09SN_06-BRANT-M1, profile station 33; seismic line 09SN_06BRANT-M2, profile station 48) are the following:

line 1			line 2		
$v_{s,5}$	=	870 m/s	$v_{s,5}$	=	921 m/s
$v_{s,10}$	=	830 m/s	$v_{s,10}$	=	836 m/s
$v_{s,20}$	=	966 m/s	$v_{s,20}$	=	908 m/s
$v_{s,30}$	=	1080 m/s	$v_{s,30}$	=	1051 m/s
$v_{s,40}$	=	1180 m/s	$v_{s,40}$	=	1150 m/s

- The estimated reliable shear wave velocity of hard rock derived by refraction tomography is 1900 m/s.
- The estimated reliable refraction compressional wave velocity of hard rock derived by refraction tomography is 3300 m/s.
- The geophysical interpretation of the subsurface structures in this report are to be validated and incorporated into a comprehensive appraisal by a geologist familiar with the local geological setting.

Schwerzenbach, 3rd July 2009

Walter Frei
dipl. Natw. ETH
managing director

Lorenz Keller
dipl. Natw. ETH
project manager